Aerospace Science and Technology 133 (2023) 108099

Contents lists available at ScienceDirect

Aerospace Science and Technology

journal homepage: www.elsevier.com/locate/aescte

Disturbance observer-based performance guaranteed fault-tolerant control for multi-spacecraft formation reconfiguration with collision avoidance

Qingxian Jia [a,*], Yule Gui [a], Yunhua Wu [a], Chengxi Zhang [b]

[a] College of Astronautics, Nanjing University of Aeronautics and Astronautics, 210016 Nanjing, China
[b] School of Internet of Things Engineering, Jiangnan University, 214122 Wuxi, China

ARTICLE INFO

Article history:
Received 27 September 2022
Received in revised form 17 November 2022
Accepted 27 December 2022
Available online 3 January 2023
Communicated by Qinglei Hu

Keywords:
Spacecraft formation flying
Disturbance observer
Artificial potential function
Collision avoidance
Performance guaranteed control
Fault-tolerant control

ABSTRACT

In this study, the issue of the performance guaranteed fault-tolerant control for formation reconfiguration with collision avoidance in the multi-spacecraft system subjects to space perturbations and thruster faults is investigated. A new nonlinear iterative learning disturbance observer is constructed to accurately reconstruct the synthesized disturbance no matter it is time-varying or not. Then, an exponential artificial potential function with a simple structure and low computation requirement is designed to avoid collision between spacecrafts. A nonsingular terminal sliding mode fault-tolerant control method is explored to accomplish fault-tolerant formation reconfiguration with collision avoidance ability and prescribed robust performance. Finally, numerical simulations and comparisons are performed to validate the effectiveness and superiority of the proposed approaches.

1. Introduction

During the past decades, Spacecraft Formation Flying (SFF) has become an increasingly attractive research topic in earth observation, high-resolution, deep space imaging and exploration [1]. Compared with a large, complex and single-purpose spacecraft, SFF system with multiple small spacecrafts has considerable advantages in space missions, such as high flexibility, low cost, shortened development cycle, and more enormous function expansion capacity [2]. In general, SFF control mainly includes formation keeping and formation reconfiguration. The formation keeping requires accurate nominal configuration maintenance under the space perturbations. Formation reconfiguration is usually required such that formation configurations can be controllably switched between each other due to the transformation of formation mission. In view to the wide application prospect of SFF system in the aerospace field, extensive studies on SFF control techniques have been devoted and fruitful achievements have been reviewed in the [3–5] and the reference therein.

In general, collision avoidance between spacecrafts is crucial in the aerospace field [6]. Especially, for the formation reconfiguration in close SFF systems, collision avoidance is a necessary concern to ensure system safety during the reconfiguration process [7]. As an effective collision avoidance method, Artificial Potential Function (APF) strategy has been widely studied, and recent great progress on APF-based collision avoidance control has been developed in [8–15]. To achieve precise formation reconfiguration, collision avoidance and uniform distribution operations simultaneously, a set of APF-based self-organizing control strategies for large-scale spacecraft swarm are presented in [8]. Literature [9] innovatively proposes a Relative Orbital Elements (ROE) and APF-based collision avoidance control algorithm. In [10], an adaptive APF-based linear quadratic regular control method is presented for spacecraft formation reconfiguration when considering navigation and control uncertainties. Based on the Nonsingular Terminal Sliding Mode (NTSM) and the APF, a coordinated controller with fixed-time observer is designed in [11] to achieve fixed-time spacecraft formation reconfiguration with collision avoidance. Based on the APF with the rotational potential, a gradient-based control law for SFF system with obstacle avoidance is proposed aiming at configuration maintenance and reconfiguration in [12]. To address different collision avoidance constraints of spacecraft swarm, autonomous reconfiguration control architecture with low computational cost is provided based on the ROE and the APF in [13]. For

* Corresponding author.
E-mail addresses: jqxnuaa@nuaa.edu.cn (Q. Jia), gylgyl@nuaa.edu.cn (Y. Gui), yunhuawu@nuaa.edu.cn (Y. Wu), dongfangxy@163.com (C. Zhang).

https://doi.org/10.1016/j.ast.2022.108099
1270-9638/

the spacecraft formation reconfiguration under input saturation, a fixed-time stable control scheme is proposed in [14] to guarantee the position tracking performance. In [15], based on the logarithmic APF method and prescribed performance control method, an integrated tracking control protocol is designed for the SFF system with external disturbance and sensing radius, such that the formation collision avoidance reconfiguration could be guaranteed. In the aforementioned literatures, thruster faults have not been focused, nevertheless, they may exist due to extremely harsh outer space environment and on-orbit long-term operation. In addition, space perturbations are usually passively considered and specific reconfiguration performance criteria have been not considered such that reconfiguration performance with collision avoidance is limited for SFF system.

Additionally, a spacecraft formation control system unavoidably manifests various types of unexpected anomalies and faults during on-orbit mission operations [16]. These factors result in performance degradation, instability, or even catastrophic outcomes [17]. Therefore, Fault-Tolerant Control (FTC) for SFF systems has been attracting considerable attention during the past decade. A linear iterative learning algorithm-based active FTC for SFF system is investigated in [18], where an Iterative Learning Observer (ILO) is proposed to accurately reconstruct thruster faults while a learning output feedback FTC approach is explored for spacecraft formation configuration maintainance. The reconstruction error and relative position control error will exist for a leader spacecraft with an elliptical orbit and a large-dimension formation configuration. In [19], a sliding-mode fault-tolerant controller is developed to guarantee high-precision formation control for SFF system with large perturbation. For accurate relative position tracking control, two adaptive FTC methods are presented in [20], where various adaptive learning algorithms are respectively adopted to update and compensate space perturbations, time-varying communication delays and parameter uncertainties. Such an operation results in massive computation consumption. A finite-time Extended State Observer (ESO)-based an adaptive fault-tolerant backstepping control law with prescribed performance is developed in [21] to handle trajectory tracking control problem for 6-DOF spacecraft proximity operations. A dimensional extension of the ESO inevitably increase the computation burden in [21]. In addition, various types of Disturbance Observers (DOs) have been applied for high-precision formation control for SFF system. In [22], a Nonlinear DO (NDO)-based asymptotic tracking control scheme is designed to achieve robust tracking performance for SFF system, but the constant disturbances are considered theoretically. In [23], an integral-type Sliding Mode Control (SMC) strategy is designed to guarantee anti-disturbances and anti-fault ability for underactuated spacecraft rendezvous. An adaptive iterative learning control method for flexible spacecraft rendezvous is developed in [24], where a PD-type Iterative Learning Disturbance Observer (ILDO) is designed to reconstruct the high-frequency periodic disturbance. However, PD-type iterative learning algorithm requires a complex updating law with excessive parameters. It is worth noting that, the issue of collision avoidance in spacecraft fault-tolerant formation control has been not focused in [18–24]. To the best of our knowledge, no results on spacecraft fault-tolerant formation control with collision avoidance ability have been developed so far. Besides, prescribed performance has never been focused when considering the influence of space perturbations and thruster faults. Therefore, there is a strong incentive for us to investigate DO-based prescribed performance FTC for multi-spacecraft formation control with collision avoidance.

Based on the aforementioned discussions, the issue of ILO-based performance guaranteed FTC for multi-spacecraft formation reconfiguration with collision avoidance is investigated in this paper. The algebraic P-type iterative learning algorithm is adopted for disturbance reconstruction in view to its low online computing power. First, we construct a nonlinear relative orbit dynamics model satisfying the Lipschitz constraint for a leader-follower SFF system. For the nonlinear relative dynamics, a new nonlinear ILDO (NILDO) is constructed to reconstruct the synthesized disturbance. The partial gain matrices of the NILDO are easily computed through Linear Matrix Inequality (LMI) optimization technique. Further, based on the exponential APF and H_∞ performance index, a robust Nonsingular Terminal Sliding Mode FTC (NTSMFTC) law is explored to achieve fast and accurate formation reconfiguration with fault-tolerant ability and collision avoidance ability. The stability of the NILDO and of the NTSMFTC law are respectively proven using Lyapunov stability theory. Finally, simulation studies are performed to illustrate the effectiveness and superiority of the proposed approaches. Compared with the previous studies, the main contributions and features of this study are given as follows,

(1) Inspired by the existing ILOs [18,25], a new NILDO is explored to reconstruct the synthesized disturbance including space perturbations and thruster faults for a nonlinear leader-follower SFF formation system. Compared with the NDO [22], the proposed NILDO has faster convergence property and higher reconstruction accuracy.
(2) To achieve the collision avoidance, an exponential APF is proposed such that the distance between each spacecraft meets the requirement of predetermined safe distance. Compared with the APF proposed in [9], the proposed exponential APF has a simpler form and lower computational cost. Therefore, it is easier to be implemented when considering the limited resource of onboard computer.
(3) To achieve fast and robust fault-tolerant formation reconfiguration without collision, exponential APF-based robust NTSMFTC law is designed with a prescribed H_∞ performance index for a leader-follower SFF system subjects to space perturbations and thruster faults. Compared with the Linear SMC (LSMC) method [19] and the NTSMC [26], the proposed robust NTSMFTC law has higher control accuracy on the relative positions.

The rest of this paper is organized as follows. In Section 2, the considered nonlinear SFF system model and the main problems are stated. In Section 3, an NILDO is designed and the stability analysis of the proposed NILDO is also given in detail. In Section 4, the exponential APF-based robust NTSMFTC approach is presented for formation reconfiguration with fault-tolerant ability and collision avoidance ability. In Section 5, simulation studies are provided and Section 6 concludes this paper.

2. Dynamical equations of relative motion

This paper considers a SFF system including a virtual leader spacecraft and multiple follower spacecrafts, as depicted in Fig. 1. Let $\mathcal{L} = \{X, Y, Z\}$ denotes the Earth-Centered Inertial (ECI) frame that is fixed at the center of the earth and $\mathcal{F} = \{x, y, z\}$ represents the local vertical local horizontal coordinate frame that is attached to the center of the leader spacecraft. In Fig. 1, $\boldsymbol{r}$ refers to the position vector from Earth center to the virtual leader spacecraft, $\boldsymbol{\rho}_i \in \mathbb{R}^3$ refers to the relative position vector of the ith spacecraft with respect to the virtual leader spacecraft.

Considering thruster faults and space perturbations, the motion dynamics [27] of ith follower spacecraft relative to the leader spacecraft is modeled as

$$\begin{cases} \dot{\boldsymbol{\rho}}_i = \boldsymbol{v}_i \\ m_i \dot{\boldsymbol{v}}_i = \boldsymbol{H}_i \boldsymbol{v}_i + \boldsymbol{D}_i \boldsymbol{\rho}_i + \boldsymbol{N}_i + \boldsymbol{d}_i + \boldsymbol{f}_i + \boldsymbol{u}_i \end{cases} \tag{1}$$

where $\boldsymbol{\rho}_i = [x_i, y_i, z_i]^T$ and $\boldsymbol{v}_i = [\dot{x}_i, \dot{y}_i, \dot{z}_i]^T$ denote the relative position and relative velocity of the ith follower spacecraft re-

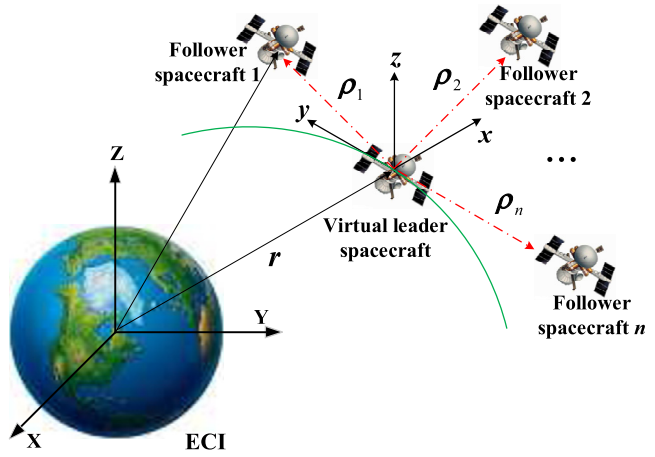

Fig. 1. The relative coordinate frames for a leader-follower SFF system.

spectively, m_i is the mass of the ith follower spacecraft, $\boldsymbol{d}_i = [d_x, d_y, d_z]^T$ is the space perturbation vector, $\boldsymbol{f}_i = [f_x, f_y, f_z]^T$ is the thruster bias fault, $\boldsymbol{u}_i = [u_x, u_y, u_z]^T$ is the control force vector. In (1), the parameter matrices can be obtained as follows,

$$\boldsymbol{H}_i(n) = m_i \begin{bmatrix} 0 & 2n & 0 \\ -2n & 0 & 0 \\ 0 & 0 & 0 \end{bmatrix},$$

$$\boldsymbol{D}_i(n, \dot{n}, r_i) = -m_i \frac{\mu}{r_i^3} \boldsymbol{I}_3 + m_i \begin{bmatrix} n^2 & \dot{n} & 0 \\ -\dot{n} & n^2 & 0 \\ 0 & 0 & 0 \end{bmatrix},$$

$$\boldsymbol{N}_i(r_i, a) = \mu m_i \left[\frac{1}{a^2} - \frac{a}{r_i^3}, 0, 0 \right]^T$$

where $r_i = \sqrt{(a + x_i)^2 + y_i^2 + z_i^2}$, μ is the gravitational coefficient of the earth, n denotes the orbital rate, a is the semi-major axis of the leader spacecraft.

Considering thruster fault as external disturbance and the nonlinear motion dynamics (1) can be rewritten into the following nonlinear state-space model:

$$\begin{cases} \dot{\boldsymbol{q}}_i(t) = \boldsymbol{A}\boldsymbol{q}_i(t) + \boldsymbol{G}_i(\boldsymbol{q}_i, t) + \boldsymbol{B}_i\boldsymbol{u}_i(t) + \boldsymbol{E}_i\boldsymbol{S}_{pfi} \\ \boldsymbol{y}_i(t) = \boldsymbol{C}\boldsymbol{q}_i(t) \end{cases} \tag{2}$$

where $\boldsymbol{q}_i(t) = [x_i, y_i, z_i, \dot{x}_i, \dot{y}_i, \dot{z}_i]^T$ represents system state including the relative positive and the relative velocity, $\boldsymbol{y}_i(t)$ represents system measurement output vector, $\boldsymbol{S}_{pfi}(t) = \boldsymbol{d}_i(t) + \boldsymbol{f}_i(t)$ representing the synthesized disturbance of the ith follower spacecraft, $\boldsymbol{G}_i(\boldsymbol{q}, t) = \begin{bmatrix} \boldsymbol{Ze} \\ \frac{\mu}{a^2} \\ 0 \\ 0 \end{bmatrix} - \frac{\mu}{r_i^3} \begin{bmatrix} \boldsymbol{Ze} \\ a + x_i \\ y_i \\ z_i \end{bmatrix}$ is the nonlinear term with $\boldsymbol{Ze} = [0, 0, 0]^T$. In (2), parameter matrices can be computed as follows,

$$\boldsymbol{A} = \begin{bmatrix} \boldsymbol{0}_3 & \boldsymbol{I}_3 \\ \boldsymbol{A}_1 & \boldsymbol{A}_2 \end{bmatrix}, \quad \boldsymbol{A}_1 = \begin{bmatrix} n^2 & \dot{n} & 0 \\ -\dot{n} & n^2 & 0 \\ 0 & 0 & 0 \end{bmatrix},$$

$$\boldsymbol{A}_2 = \begin{bmatrix} 0 & 2n & 0 \\ -2n & 0 & 0 \\ 0 & 0 & 0 \end{bmatrix}, \quad \boldsymbol{B}_i = \boldsymbol{E}_i = \frac{1}{m_i} \begin{bmatrix} \boldsymbol{0}_3 \\ \boldsymbol{I}_3 \end{bmatrix}, \quad \boldsymbol{C} = \boldsymbol{I}_6.$$

To present the main results, the following assumptions are made.

Assumption 1. The space perturbation $\boldsymbol{d}_i$ is assumed to be unknown but bounded, which satisfies

$$\left\| \boldsymbol{d}_i(t) \right\| \leq d_{\max} \tag{3}$$

Assumption 2. [28]. The nonlinear term $\boldsymbol{G}(\boldsymbol{q}, t)$ is locally Lipschitz about $\boldsymbol{q}$ uniformly, e.g.,

$$\left\| \boldsymbol{G}(\boldsymbol{q}_1, t) - \boldsymbol{G}(\boldsymbol{q}_2, t) \right\| \leq L_g \| \boldsymbol{q}_1 - \boldsymbol{q}_2 \| \tag{4}$$

where L_g is the Lipschitz constant.

Remark 1. The space perturbation mainly includes earth gravitational field perturbation force, atmospheric drag, and solar radiation perturbation, etc, such that Assumption 1 is reasonable in practice [29,30]. It is worth mentioning that similar assumptions can be found in [31] and the reference therein. Assumption 2 gives a limitation on the nonlinear term $\boldsymbol{G}(\boldsymbol{q}, t)$, whose change is very small due to the small orbit rate. It implies that Assumption 2 is feasible.

The prime purpose of this work is to achieve accurate, rapid performance guaranteed fault-tolerant formation reconfiguration with collision avoidance for multi-spacecraft system. Based on our previous results on the ILO design [18,25], an NILDO is explored for (2) to reconstruct the synthesized disturbance $\boldsymbol{S}_{pfi}(t)$. Based on the exponential APF and the NTSMC method, an NTSMFTC with preassigned H_∞ performance is presented for (2) to achieve robust and accurate multi-spacecraft formation reconfiguration without collision.

3. NILDO-based synthesized disturbance reconstruction approach

In this section, a continuous-time NILDO is constructed to reconstruct the synthesized disturbance, and the stability analysis of the NILDO is explicitly given.

3.1. Design of the nonlinear iterative learning disturbance observer

To reconstruct the synthesized disturbance in the ith SFF system, a continuous-time NILDO is constructed for (2) as follows,

$$\begin{cases} \dot{\hat{\boldsymbol{q}}}_i(t) = \boldsymbol{A}\hat{\boldsymbol{q}}_i + \boldsymbol{G}(\hat{\boldsymbol{q}}_i, t) + \boldsymbol{B}_i\boldsymbol{u}_i(t) + \boldsymbol{E}_i\hat{\boldsymbol{S}}_{pfi}(t) + \boldsymbol{L}_i\boldsymbol{e}_{yi}(t) \\ \hat{\boldsymbol{y}}_i(t) = \boldsymbol{C}\hat{\boldsymbol{q}}_i(t) \\ \boldsymbol{e}_{yi}(t) = \boldsymbol{y}_i(t) - \hat{\boldsymbol{y}}_i(t) \\ \hat{\boldsymbol{S}}_{pfi}(t) = \boldsymbol{Q}_i\hat{\boldsymbol{S}}_{pfi}(t - \tau) + \boldsymbol{K}_i\boldsymbol{e}_{yi}(t) \end{cases} \tag{5}$$

where $\hat{\boldsymbol{q}}_i \in \mathbb{R}^6$ denotes the state estimation composed of the relative position estimation and relative velocity estimation, $\hat{\boldsymbol{y}}_i \in \mathbb{R}^6$ and $\boldsymbol{e}_{yi} \in \mathbb{R}^6$ are the measurement output vector and output estimation error respectively, $\hat{\boldsymbol{S}}_{pfi}(t)$ denotes the synthesized disturbance reconstruction vector, which is updated by both its previous information at $t - \tau$ and current output estimation error. Parameter τ is the learning interval, which can be taken as the simulation step, or as its integer multiple in sampled-data spacecraft control systems. Diagonal matrix $\boldsymbol{Q}_i = \text{diag}\{\alpha_1, \alpha_2, \alpha_3\}$ with $\alpha_i \in (0, 1]$, $\boldsymbol{L}_i \in \mathbb{R}^{6\times6}$ and $\boldsymbol{K}_i \in \mathbb{R}^{3\times6}$ are observer gain matrices to be determined later.

Denote state estimation error and disturbance reconstruction error as $\boldsymbol{e}_{qi}(t) = \boldsymbol{q}_i(t) - \hat{\boldsymbol{q}}_i(t)$ and $\boldsymbol{e}_{\boldsymbol{S}_{pfi}}(t) = \boldsymbol{S}_{pfi}(t) - \hat{\boldsymbol{S}}_{pfi}(t)$, respectively. As such, it follows that

$$\begin{cases} \dot{\boldsymbol{e}}_{\boldsymbol{q}i}(t) = (\boldsymbol{A} - \boldsymbol{L}_i\boldsymbol{C})\boldsymbol{e}_{\boldsymbol{q}i}(t) + \boldsymbol{E}_i\boldsymbol{e}_{\boldsymbol{S}_{pfi}}(t) + \boldsymbol{G}(\boldsymbol{q}_i, t) - \boldsymbol{G}(\hat{\boldsymbol{q}}_i, t) \\ \boldsymbol{e}_{\boldsymbol{y}i}(t) = \boldsymbol{C}\boldsymbol{e}_{\boldsymbol{q}i}(t) \end{cases} \tag{6}$$

Further, disturbance-reconstructing error $\boldsymbol{e}_{\boldsymbol{S}_{pfi}}(t)$ has the following form,

$$\begin{aligned}\boldsymbol{e}_{\boldsymbol{S}_{pfi}}(t) &= \boldsymbol{S}_{pfi}(t) - \boldsymbol{Q}_i\hat{\boldsymbol{S}}_{pfi}(t-\tau) - \boldsymbol{K}_i\boldsymbol{e}_{yi}(t) \\ &\quad + \boldsymbol{Q}_i\boldsymbol{S}_{pfi}(t-\tau) - \boldsymbol{Q}_i\boldsymbol{S}_{pfi}(t-\tau) \\ &= \boldsymbol{Q}_i\boldsymbol{e}_{\boldsymbol{S}_{pfi}}(t-\tau) - \boldsymbol{K}_i\boldsymbol{C}\boldsymbol{e}_{\boldsymbol{q}i}(t) + \tilde{\boldsymbol{S}}_{pfi}(t)\end{aligned} \tag{7}$$

where $\tilde{\boldsymbol{S}}_{pfi}(t) = \boldsymbol{S}_{pfi}(t) - \boldsymbol{Q}_i\boldsymbol{S}_{pfi}(t-\tau)$.

3.2. Stability analysis of the nonlinear iterative learning disturbance observer

Before proving the stability and convergence of the proposed NILDO, the following lemma is given.

Lemma 1. *[32]. If the Assumption 2 holds, there exists a positive-definite symmetric matrix $\boldsymbol{P}$ satisfying*

$$2\boldsymbol{e}_{\boldsymbol{q}}^T\boldsymbol{P}\big[\boldsymbol{G}(\boldsymbol{q},t) - \boldsymbol{G}(\hat{\boldsymbol{q}},t)\big] \le L_g^2\boldsymbol{e}_{\boldsymbol{q}}^T\boldsymbol{P}^T\boldsymbol{P}\boldsymbol{e}_{\boldsymbol{q}} + \boldsymbol{e}_{\boldsymbol{q}}^T\boldsymbol{e}_{\boldsymbol{q}} \tag{8}$$

Based on the above assumptions and Lemma 1, the first main result of this work is provided in the following.

Theorem 1. *. Consider the SFF system which is governed by (2) with Assumptions 1 and 2, if there exists positive-definite symmetric matrices $\boldsymbol{P}_i \in \mathbb{R}^{6\times6}$, $\boldsymbol{Q}_i \in \mathbb{R}^{3\times3}$, matrices $\boldsymbol{Y}_i \in \mathbb{R}^{6\times6}$, $\boldsymbol{K}_i \in \mathbb{R}^{3\times6}$, and a positive scalar ϑ_i such that the following conditions are satisfied,*

$$\boldsymbol{A}^T\boldsymbol{P}_i + \boldsymbol{P}_i\boldsymbol{A} - \boldsymbol{Y}_i\boldsymbol{C}_i - \boldsymbol{C}_i^T\boldsymbol{Y}_i^T + L_{gi}^2\boldsymbol{P}_i^T\boldsymbol{P}_i + \boldsymbol{I}_6 < 0 \tag{9}$$

$$\boldsymbol{P}_i\boldsymbol{E}_i = (\boldsymbol{K}_i\boldsymbol{C})^T \tag{10}$$

$$(1+\vartheta_i)\boldsymbol{Q}_i^T\boldsymbol{Q}_i - \boldsymbol{I}_6 < 0 \tag{11}$$

then the state estimation error $\boldsymbol{e}_{qi}(t)$ and disturbance-reconstructing error $\boldsymbol{e}_{\boldsymbol{S}_{pfi}}(t)$ are simultaneously uniformly ultimately bounded, and gain matrix $\boldsymbol{L}_i$ can be determined by $\boldsymbol{L}_i = \boldsymbol{P}_i^{-1}\boldsymbol{Y}_i$.

Proof. Consider the following Lyapunov function candidate:

$$V_i = \boldsymbol{e}_{qi}^T(t)\boldsymbol{P}_i\boldsymbol{e}_{qi}(t) + \int_{t-\tau}^{t}\boldsymbol{e}_{\boldsymbol{S}_{pfi}}^T(\varsigma)\boldsymbol{e}_{\boldsymbol{S}_{pfi}}(\varsigma)d\varsigma \tag{12}$$

The derivative of V with respect to time can be derived as

$$\begin{aligned}\dot{V}_i(t) &= \boldsymbol{e}_{qi}^T\big[(\boldsymbol{A}-\boldsymbol{L}_i\boldsymbol{C})^T\boldsymbol{P}_i + \boldsymbol{P}_i(\boldsymbol{A}-\boldsymbol{L}_i\boldsymbol{C})\big]\boldsymbol{e}_{qi} + 2\boldsymbol{e}_{qi}^T\boldsymbol{P}_i\boldsymbol{E}_i\boldsymbol{e}_{\boldsymbol{S}_{pfi}} \\ &\quad + 2\boldsymbol{e}_{qi}^T\boldsymbol{P}_i\big[\boldsymbol{G}(\boldsymbol{q}_i,t) - \boldsymbol{G}(\hat{\boldsymbol{q}}_i,t)\big] + \boldsymbol{e}_{\boldsymbol{S}_{pfi}}^T(t)\boldsymbol{e}_{S_{pfi}}(t) \\ &\quad - \boldsymbol{e}_{\boldsymbol{S}_{pfi}}^T(t-\tau)\boldsymbol{e}_{\boldsymbol{S}_{pfi}}(t-\tau)\end{aligned} \tag{13}$$

Substituting (7) and (8) into (13) leads to

$$\begin{aligned}\dot{V}_i(t) &\le \boldsymbol{e}_{qi}^T\big[(\boldsymbol{A}-\boldsymbol{L}_i\boldsymbol{C})^T\boldsymbol{P}_i + \boldsymbol{P}_i(\boldsymbol{A}-\boldsymbol{L}_i\boldsymbol{C}) + L_{gi}^2\boldsymbol{P}_i^T\boldsymbol{P}_i + \boldsymbol{I}_6\big]\boldsymbol{e}_{qi} \\ &\quad + 2\boldsymbol{e}_{qi}^T\boldsymbol{P}_i\boldsymbol{E}_i\big[\boldsymbol{Q}_i\boldsymbol{e}_{\boldsymbol{S}_{pfi}}(t-\tau) - \boldsymbol{K}_i\boldsymbol{C}\boldsymbol{e}_{qi}(t) + \tilde{\boldsymbol{S}}_{pfi}(t)\big] \\ &\quad + \boldsymbol{e}_{\boldsymbol{S}_{pfi}}^T(t)\boldsymbol{e}_{\boldsymbol{S}_{pfi}}(t) - \boldsymbol{e}_{\boldsymbol{S}_{pfi}}^T(t-\tau)\boldsymbol{e}_{\boldsymbol{S}_{pfi}}(t-\tau)\end{aligned} \tag{14}$$

Further, it is easily obtained from (7) that

$$\begin{aligned}\boldsymbol{e}_{\boldsymbol{S}_{pfi}}^T(t)\boldsymbol{e}_{\boldsymbol{S}_{pfi}}(t) &= \boldsymbol{e}_{\boldsymbol{S}_{pfi}}^T(t-\tau)\boldsymbol{Q}_i^T\boldsymbol{Q}_i\boldsymbol{e}_{\boldsymbol{S}_{pfi}}(t-\tau) \\ &\quad + 2\boldsymbol{e}_{qi}^T(t)(-\boldsymbol{K}_i\boldsymbol{C})^T\boldsymbol{Q}_i\boldsymbol{e}_{\boldsymbol{S}_{pfi}}(t-\tau) \\ &\quad + 2\boldsymbol{e}_{qi}^T(-\boldsymbol{K}_i\boldsymbol{C})^T\tilde{\boldsymbol{S}}_{pfi}(t) \\ &\quad + 2\boldsymbol{e}_{\boldsymbol{S}_{pfi}}^T(t-\tau)\boldsymbol{Q}_i^T\tilde{\boldsymbol{S}}_{pfi}(t) \\ &\quad + \boldsymbol{e}_{qi}^T(t)(-\boldsymbol{K}_i\boldsymbol{C})^T(-\boldsymbol{K}_i\boldsymbol{C})\boldsymbol{e}_{qi}(t) + \tilde{\boldsymbol{S}}_{pfi}^T(t)\tilde{\boldsymbol{S}}_{pfi}(t)\end{aligned} \tag{15}$$

With the help of (15), (14) can be further transformed into:

$$\begin{aligned}\dot{V}_i(t) &\le \boldsymbol{e}_{\boldsymbol{q}i}^T\big[(\boldsymbol{A}-\boldsymbol{L}_i\boldsymbol{C})^T\boldsymbol{P}_i + \boldsymbol{P}_i(\boldsymbol{A}-L_i\boldsymbol{C}) + L_{gi}^2\boldsymbol{P}_i^T\boldsymbol{P}_i + \boldsymbol{I}_6\big]\boldsymbol{e}_{\boldsymbol{q}i} \\ &\quad + \boldsymbol{e}_{\boldsymbol{S}_{pfi}}^T(t-\tau)\boldsymbol{Q}_i^T\boldsymbol{Q}_i\boldsymbol{e}_{\boldsymbol{S}_{pfi}}(t-\tau) \\ &\quad + 2\boldsymbol{e}_{\boldsymbol{q}i}^T\big[\boldsymbol{P}_i\boldsymbol{E}_i - (\boldsymbol{K}_i\boldsymbol{C})^T\big]\boldsymbol{Q}_i\boldsymbol{e}_{\boldsymbol{S}_{pfi}}(t-\tau) \\ &\quad - \boldsymbol{e}_{\boldsymbol{q}i}^T\big[2\boldsymbol{P}_i\boldsymbol{E}_i - (\boldsymbol{K}_i\boldsymbol{C})^T\big]\boldsymbol{K}_i\boldsymbol{C}\boldsymbol{e}_{\boldsymbol{q}i}(t) \\ &\quad + 2\boldsymbol{e}_{\boldsymbol{q}i}^T\big[\boldsymbol{P}_i\boldsymbol{E}_i - (\boldsymbol{K}_i\boldsymbol{C})^T\big]\tilde{\boldsymbol{S}}_{pfi}(t) \\ &\quad + 2\boldsymbol{e}_{\boldsymbol{S}_{pfi}}^T(t-\tau)\boldsymbol{Q}_i^T\tilde{\boldsymbol{S}}_{pfi}(t) + \tilde{\boldsymbol{S}}_{pfi}^T(t)\tilde{\boldsymbol{S}}_{pfi}(t) \\ &\quad - \boldsymbol{e}_{\boldsymbol{S}_{pfi}}^T(t-\tau)\boldsymbol{e}_{\boldsymbol{S}_{pfi}}(t-\tau)\end{aligned} \tag{16}$$

Under condition (10), (16) can be simplified into

$$\begin{aligned}\dot{V}_i(t) &\le \boldsymbol{e}_{qi}^T\big[(\boldsymbol{A}-\boldsymbol{L}_i\boldsymbol{C})^T\boldsymbol{P}_i + \boldsymbol{P}_i(\boldsymbol{A}-\boldsymbol{L}_i\boldsymbol{C}) + \boldsymbol{L}_{gi}^2\boldsymbol{P}_i^T\boldsymbol{P}_i + \boldsymbol{I}_6\big]\boldsymbol{e}_{qi} \\ &\quad + \boldsymbol{e}_{\boldsymbol{S}_{pfi}}^T(t-\tau)\boldsymbol{Q}_i^T\boldsymbol{Q}_i\boldsymbol{e}_{\boldsymbol{S}_{pfi}}(t-\tau) \\ &\quad + 2\boldsymbol{e}_{\boldsymbol{S}_{pfi}}^T(t-\tau)\boldsymbol{Q}_i^T\tilde{\boldsymbol{S}}_{pfi}(t) \\ &\quad + \tilde{\boldsymbol{S}}_{pfi}^T(t)\tilde{\boldsymbol{S}}_{pfi}(t) - \boldsymbol{e}_{\boldsymbol{S}_{pfi}}^T(t-\tau)\boldsymbol{e}_{\boldsymbol{S}_{pfi}}(t-\tau)\end{aligned} \tag{17}$$

According to the Young's inequality [33], one further has

$$\begin{aligned}&2\boldsymbol{e}_{\boldsymbol{S}_{pfi}}^T(t-\tau)\boldsymbol{Q}_i^T\tilde{\boldsymbol{S}}_{pfi}(t) \\ &\le \vartheta_i\boldsymbol{e}_{\boldsymbol{S}_{pfi}}^T(t-\tau)\boldsymbol{Q}_i^T\boldsymbol{Q}_i\boldsymbol{e}_{\boldsymbol{S}_{pfi}}(t-\tau) + \frac{1}{\vartheta_i}\tilde{\boldsymbol{S}}_{pfi}^T(t)\tilde{\boldsymbol{S}}_{pfi}(t)\end{aligned} \tag{18}$$

With the help of (18), (17) is further transformed into

$$\begin{aligned}\dot{V}_i(t) &\le \boldsymbol{e}_{qi}^T\big[(\boldsymbol{A}-\boldsymbol{L}_i\boldsymbol{C})^T\boldsymbol{P}_i + \boldsymbol{P}_i(\boldsymbol{A}-\boldsymbol{L}_i\boldsymbol{C}) + L_{gi}^2\boldsymbol{P}_i^T\boldsymbol{P}_i + \boldsymbol{I}_6\big]\boldsymbol{e}_{qi} \\ &\quad + \boldsymbol{e}_{\boldsymbol{S}_{pfi}}^T(t-\tau)\big[(1+\vartheta_i)\boldsymbol{Q}_i^T\boldsymbol{Q}_i - \boldsymbol{I}_6\big]\boldsymbol{e}_{\boldsymbol{S}_{pfi}}(t-\tau) \\ &\quad + \left(1+\frac{1}{\vartheta_i}\right)\tilde{\boldsymbol{S}}_{pfi}^T(t)\tilde{\boldsymbol{S}}_{pfi}(t)\end{aligned} \tag{19}$$

Define the left siding of (9) and (11) as $\boldsymbol{\Omega}$ and $\boldsymbol{\Pi}$, respectively. If conditions (9) and (11) hold, we have

$$\dot{V}_i(t) \le -\lambda_{\min}(\boldsymbol{\Omega})\|\boldsymbol{e}_{qi}\|^2 - \lambda_{\min}(\boldsymbol{\Pi})\big\|e_{\boldsymbol{S}_{pfi}}(t-\tau)\big\|^2 + \nu \tag{20}$$

where $\nu = (1+\frac{1}{\vartheta_i})\tilde{\boldsymbol{S}}_{pfi}^T(t)\tilde{\boldsymbol{S}}_{pfi}(t)$. If Assumption 1 holds and thruster faults are bounded, uniform ultimate boundedness of $\boldsymbol{e}_{qi}(t)$ and $\boldsymbol{e}_{\boldsymbol{S}_{pfi}}(t-\tau)$ can be thus guaranteed according to (20). This completes the proof. □

Remark 2. To calculate gain matrices $\boldsymbol{L}_i$ and $\boldsymbol{K}_i$, the matrix inequality (9) is equivalently converted into

$$\begin{bmatrix}\boldsymbol{A}^T\boldsymbol{P}_i + \boldsymbol{P}_i\boldsymbol{A} - \boldsymbol{Y}_i\boldsymbol{C} - \boldsymbol{C}^T\boldsymbol{Y}_i^T + \boldsymbol{I}_6 & \boldsymbol{L}_{gi}\boldsymbol{P}_i \\ * & -\boldsymbol{I}_6\end{bmatrix} < 0 \tag{21}$$

In addition, the problem of solving (10) is transformed into one of solving the following matrix inequality [25]

$$\begin{bmatrix}-\varpi\boldsymbol{I}_3 & \boldsymbol{E}_i^T\boldsymbol{P}_i - \boldsymbol{K}_i\boldsymbol{C} \\ * & -\boldsymbol{I}_6\end{bmatrix} < 0 \tag{22}$$

where ϖ is a positive scalar. Therefore, matrices $\boldsymbol{L}_i$ and $\boldsymbol{K}_i$ can be obtained by solving (21) and (22) using the solver *feasp* or *mincx* in the MATLAB/LMI toolbox.

Remark 3. In [22], NDO-based disturbance reconstruction is developed based on the assumption that external disturbance is constant or slowly time-varying. Compared with the NDO method [22], such an assumption is not required for the proposed NILDO such that the synthesized disturbance can be reconstructed no

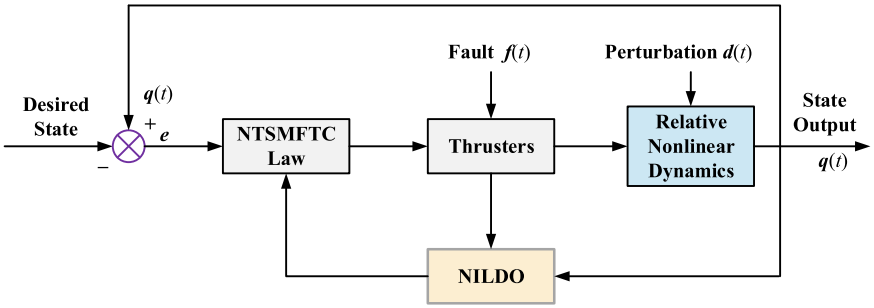

Fig. 2. The block diagram of spacecraft formation reconfiguration control scheme.

matter it is constant or time-varying. In addition, compared with the PD-type ILDO design [24], the proposed NILDO possesses a simpler updating law with less parameter matrices, and it thus requires less computation consumption. Therefore, the proposed NILDO have a wilder applicable scope for SFF systems.

Remark 4. It is worth noting that ILO-based disturbance reconstruction and attitude FTC have been widely studied for single spacecraft in [31,34–36] and other literature therein. However, few researches have been devoted to the issue of ILO-based disturbance reconstruction (or fault) and formation FTC for SFF systems, which is also the main motivation of our paper.

Following Theorem 1, a design procedure for the presented NILDO is given as follows,

Design procedure for the presented NILDO	
1.	Select small positive scalars ϑ_i, then compute $\boldsymbol{Q}_i$ through solving (11).
2.	Choose a sufficiently small parameter ϖ, then matrices $\boldsymbol{P}_i$, $\boldsymbol{Y}_i$ and $\boldsymbol{K}_i$ can be calculated through solving (21) and (22) using the Matlab/LMI toolbox.
3.	Compute the gain matrix $\boldsymbol{L}_i$ by solving $\boldsymbol{L}_i = \boldsymbol{P}_i^{-1}\boldsymbol{Y}_i$.
4.	Select the appropriate learning interval τ according to the simulation step.

4. Nonsingular terminal sliding mode fault-tolerant control for multi-spacecraft formation reconfiguration

In this section, based on the exponential APF and guaranteed H_∞ performance, a robust NTSMFTC approach is explored such that precise and fast multi-spacecraft fault-tolerant formation reconfiguration without collision can be guaranteed in the presence of space perturbations and thruster faults. The block diagram of the proposed NILDO and NTSMFTC law-based spacecraft formation reconfiguration control scheme is shown in Fig. 2.

4.1. The artificial potential function construction

Inspired by [9], a new APF of ith and jth spacecraft is constructed as follow,

$$J_{ij} = e^{-\Upsilon(d_{ij}-M_d)} \tag{23}$$

where $\Upsilon > 0$ denotes a weight coefficient, $d_{ij} = \|\boldsymbol{\rho}_i - \boldsymbol{\rho}_j\|$ is the space distance between ith spacecraft and jth spacecraft, M_d is the predetermined safe distance between spacecrafts. It can be noted that the potential function J_{ij} is differentiable and it approaches to zero when d_{ij} is larger than M_d.

It is assumed that safe distance $M_d = 5$ m, the relationship between the value of APF and the relative position of spacecrafts is shown in Fig. 3. From Fig. 3(a)-(c), it can be seen that APF has high values when the distances between spacecrafts are less than the safe distance. Contrarily, the APF has global minimum at the safe position of the spacecrafts. The above result can be obtained from the curve of APF with respect to space distance d_{ij} in Fig. 3(d). About the potential surface for APF, the interesting reader can be also referred to [37] and the reference therein.

Define an auxiliary variable $\boldsymbol{\psi}_i = \sum_{j=1}^{N} \frac{\partial J_{ij}}{\partial \rho_i}$, then one can obtain

$$\boldsymbol{\psi}_i = \sum_{j=1}^{N} \begin{bmatrix} \psi_{ix} \\ \psi_{iy} \\ \psi_{iz} \end{bmatrix} = \sum_{j=1}^{N} \begin{bmatrix} \frac{-\Upsilon e^{-\Upsilon(d_{ij}-M_d)}(x_i - x_j)}{d_{ij}} \\ \frac{-\Upsilon e^{-\Upsilon(d_{ij}-M_d)}(y_i - y_j)}{d_{ij}} \\ \frac{-\Upsilon e^{-\Upsilon(d_{ij}-M_d)}(z_i - z_j)}{d_{ij}} \end{bmatrix} \tag{24}$$

where N is the number of spacecrafts in formation.

Assumption 3. [37] The first derivative of $\boldsymbol{\psi}_i$ with respect to time is assumed to be bounded, e.g.,

$$m_i \left\| \frac{d\boldsymbol{\psi}_i}{dt} \right\| \leq \kappa_1 \tag{25}$$

where κ_1 is a positive scalar.

Remark 5. It should be pointed out that the relative velocity of the ith spacecraft relative to the reference spacecraft is bounded in practice. In addition, the distance between the follower spacecrafts is limited during the formation configuration process. Therefore, it is reasonable for Assumption 3 in practice.

Remark 6. Compared with the exponential APFs for collision avoidance proposed in [9] and [10], the designed new exponential APF has a simpler form and less calculation burden. In addition, this function contains a safe distance term such that the distance between each spacecraft satisfies the requirement of any predetermined safe distance in the process of formation reconfiguration. The APF proposed in [12] could circumvent local minima due to a rotational potential, but it also requires a more complex structure with more parameters. Additionally, the SFF system represented using linear C-W model is only focused, and the FTC issue is not considered in [10] and [12].

4.2. Design of the nonsingular terminal sliding mode fault-tolerant control

Based on the synthesized disturbance signal obtained from the NILDO (5), the relative motion of the ith spacecraft (2) can be rewritten as follows,

$$\begin{cases} \dot{\boldsymbol{\rho}}_i = \boldsymbol{v}_i \\ m_i \dot{\boldsymbol{v}}_i = \boldsymbol{H}_i \boldsymbol{v}_i + \boldsymbol{D}_i \boldsymbol{\rho}_i + \boldsymbol{N}_i + \boldsymbol{e}_{\boldsymbol{S}_{pfi}} + \hat{\boldsymbol{S}}_{pfi} + \boldsymbol{u}_i \end{cases} \tag{26}$$

where $\boldsymbol{e}_{\boldsymbol{S}_{pfi}}(t) = \boldsymbol{S}_{pfi}(t) - \hat{\boldsymbol{S}}_{pfi}(t)$ representing disturbance reconstruction error.

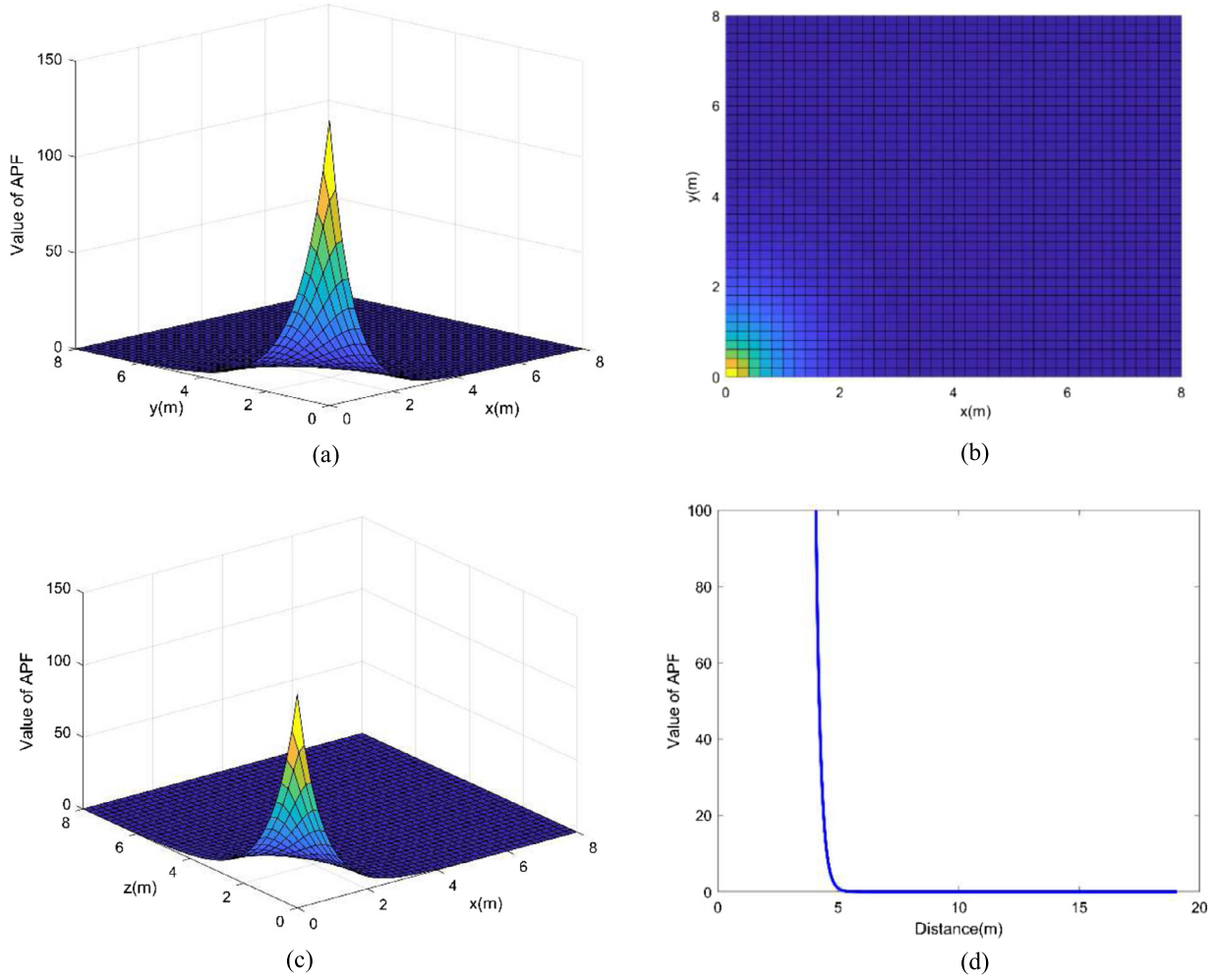

Fig. 3. The potential surface of the artificial potential function.

Define $\boldsymbol{\rho}_{id}$ and $\dot{\boldsymbol{\rho}}_{id}$ as the desired position and velocity of the ith follower spacecraft in target configuration. Then $\boldsymbol{e}_{\boldsymbol{\rho}i} = \boldsymbol{\rho}_i - \boldsymbol{\rho}_{id}$ and $\boldsymbol{e}_{\boldsymbol{v}i} = \dot{\boldsymbol{\rho}}_i - \dot{\boldsymbol{\rho}}_{id}$ denote the position tracking error and velocity tracking error respectively.

To achieve fast and accurate formation reconfiguration without collision in the presence of space perturbations and thruster faults, an exponential APF-based NTSM surface [38] is suggested as follows,

$$\boldsymbol{s}_i = \boldsymbol{e}_{\boldsymbol{\rho}i} + \varepsilon_1 \mathrm{sig}^{\gamma_1}(\boldsymbol{e}_{\boldsymbol{\rho}i}) + \varepsilon_2 \mathrm{sig}^{\gamma_2}(\boldsymbol{e}_{\boldsymbol{v}i}) + \boldsymbol{\psi}_i \tag{27}$$

where $\gamma_1 > \gamma_2$, $1 < \gamma_2 < 2$, $\varepsilon_1 > 0$ and $\varepsilon_2 > 0$. The terms $\mathrm{sig}^{\gamma_1}(\boldsymbol{e}_{\boldsymbol{\rho}i})$ and $\mathrm{sig}^{\gamma_2}(\boldsymbol{e}_{\boldsymbol{v}i})$ are defined as follows,

$$\mathrm{sig}^{\gamma_1}(\boldsymbol{e}_{\boldsymbol{\rho}i}) = \left[|e_{\rho ix}|^{\gamma_1}\,\mathrm{sign}(e_{\rho ix}), |e_{\rho iy}|^{\gamma_1}\,\mathrm{sign}(e_{\rho iy}), |e_{\rho iz}|^{\gamma_1}\,\mathrm{sign}(e_{\rho iz})\right]^T$$

and

$$\mathrm{sig}^{\gamma_2}(\boldsymbol{e}_{\boldsymbol{v}i}) = \left[|e_{vix}|^{\gamma_2}\,\mathrm{sign}(e_{vix}), |e_{viy}|^{\gamma_2}\,\mathrm{sign}(e_{viy}), |e_{viz}|^{\gamma_2}\,\mathrm{sign}(e_{viz})\right]^T.$$

The derivative of $\boldsymbol{s}_i$ can be written as

$$\dot{\boldsymbol{s}}_i = \boldsymbol{e}_{vi} + \varepsilon_1\gamma_1 \boldsymbol{R}_i \boldsymbol{e}_{vi} + \varepsilon_2\gamma_2 \boldsymbol{W}_i \dot{\boldsymbol{e}}_{vi} + \dot{\boldsymbol{\psi}}_i \tag{28}$$

where $\boldsymbol{R}_i = \mathrm{diag}\{|e_{\rho ix}|^{\gamma_1-1}, |e_{\rho iy}|^{\gamma_1-1}, |e_{\rho iz}|^{\gamma_1-1}\}$, $\boldsymbol{W}_i = \mathrm{diag}\{|e_{vix}|^{\gamma_2-1}, |e_{viy}|^{\gamma_2-1}, |e_{viz}|^{\gamma_2-1}\}$.

Based on the above NTSM surface, the second main result of this paper is summarized in the following.

Theorem 2. *Consider the ith follower spacecraft's formation dynamics (26) under Assumption 3, an NTSMFTC law is designed as follows,*

$$\boldsymbol{u}_i = \boldsymbol{u}_{1i} + \boldsymbol{u}_{2i} + \boldsymbol{u}_{3i} \tag{29}$$

with

$$\boldsymbol{u}_{1i} = -\delta_i(t)\boldsymbol{s}_i - \frac{\kappa_1 \boldsymbol{W}_i^{-1}\,\mathrm{sign}(\boldsymbol{s}_i)}{\varepsilon_2\gamma_2} - \frac{m_i \boldsymbol{W}_i^{-1}\boldsymbol{e}_{vi}}{\varepsilon_2\gamma_2} - \frac{m_i\varepsilon_1\gamma_1 \boldsymbol{W}_i^{-1}\boldsymbol{R}_i\boldsymbol{e}_{vi}}{\varepsilon_2\gamma_2} + m_i\ddot{\boldsymbol{\rho}}_{id},$$

$$\boldsymbol{u}_{2i} = -\boldsymbol{H}_i\boldsymbol{v}_i - \boldsymbol{D}_i\boldsymbol{\rho}_i - \boldsymbol{N}_i, \qquad \boldsymbol{u}_{3i} = -\hat{\boldsymbol{S}}_{\boldsymbol{pf}i},$$

where $\boldsymbol{\delta}_i = \mathrm{diag}\{\delta_{ix}, \delta_{iy}, \delta_{iz}\}$ is a positive definite diagonal matrix. If the following condition is satisfied,

$$\begin{bmatrix} \boldsymbol{I}_3 - \varepsilon_2\gamma_2 \boldsymbol{W}_i\delta_i & \frac{1}{2}\varepsilon_2\gamma_2 \boldsymbol{W}_i \\ (\frac{1}{2}\varepsilon_2\gamma_2 \boldsymbol{W}_i)^T & -\xi \boldsymbol{I}_3 \end{bmatrix} < 0 \tag{30}$$

then the designed NTSMFTC law (29) can guarantee that the tracking errors $\boldsymbol{e}_{\boldsymbol{\rho}i}$ and $\boldsymbol{e}_{\boldsymbol{v}i}$ are robust stable, and the following H_∞ performance constraint can be satisfied that

$$\sum_{i=1}^{N}\int_0^{\infty}\boldsymbol{s}_i^T(t)\boldsymbol{s}_i(t)dt \le \xi\sum_{i=1}^{N}\int_0^{\infty}\boldsymbol{e}_{\boldsymbol{S}_{pfi}}^T(t)\boldsymbol{e}_{\boldsymbol{S}_{pfi}}(t)dt,\quad \xi>0 \tag{31}$$

Proof. Consider the following Lyapunov function candidate

$$V=\frac{1}{2}\sum_{i=1}^{N}\boldsymbol{s}_i^T m_i\boldsymbol{s}_i \tag{32}$$

There are two main steps in the following proof.

Step 1: The stability proof of the designed NTSMFTC law. The time derivative of V is calculated as

$$\begin{aligned}\dot{V}&=\sum_{i=1}^{N}\boldsymbol{s}_i^T m_i\dot{\boldsymbol{s}}_i\\&=\sum_{i=1}^{N}\boldsymbol{s}_i^T m_i(\boldsymbol{e}_{\boldsymbol{v}i}+\varepsilon_1\gamma_1\boldsymbol{R}_i\boldsymbol{e}_{\boldsymbol{v}i}+\varepsilon_2\gamma_2\boldsymbol{W}_i\dot{\boldsymbol{e}}_{\boldsymbol{v}i}+\dot{\boldsymbol{\psi}}_i)\\&=\sum_{i=1}^{N}\boldsymbol{s}_i^T\left(m_i\boldsymbol{e}_{\boldsymbol{v}i}+m_i\varepsilon_1\gamma_1\boldsymbol{R}_i\boldsymbol{e}_{\boldsymbol{v}i}+m_i\varepsilon_2\gamma_2\boldsymbol{W}_i(\ddot{\boldsymbol{\rho}}_i-\ddot{\boldsymbol{\rho}}_{id})+m_i\dot{\boldsymbol{\psi}}_i\right)\\&=\sum_{i=1}^{N}\boldsymbol{s}_i^T\big[m_i\boldsymbol{e}_{\boldsymbol{v}i}+m_i\varepsilon_1\gamma_1\boldsymbol{R}_i\boldsymbol{e}_{\boldsymbol{v}i}\\&\quad+\varepsilon_2\gamma_2\boldsymbol{W}_i(\boldsymbol{H}_i\boldsymbol{v}_i+\boldsymbol{D}_i\boldsymbol{\rho}_i+\boldsymbol{N}_i+\boldsymbol{S}_{\boldsymbol{p}\boldsymbol{f}i}+\boldsymbol{u}_i)\\&\quad-m_i\varepsilon_2\gamma_2\boldsymbol{W}_i\ddot{\boldsymbol{\rho}}_{id}+m_i\dot{\boldsymbol{\psi}}_i\big]\end{aligned} \tag{33}$$

Substituting (29) into (33) yields

$$\dot{V}=\sum_{i=1}^{N}\boldsymbol{s}_i^T\left[-\varepsilon_2\gamma_2\boldsymbol{W}_i\delta_i\boldsymbol{s}_i+\varepsilon_2\gamma_2\boldsymbol{W}_i\boldsymbol{e}_{\boldsymbol{S}_{pfi}}-\kappa_1\,\mathrm{sign}(\boldsymbol{s}_i)+m_i\dot{\boldsymbol{\psi}}_i\right] \tag{34}$$

According to Assumption 3, we can obtain

$$\begin{aligned}\dot{V}&\le\sum_{i=1}^{N}\boldsymbol{s}_i^T(-\varepsilon_2\gamma_2\boldsymbol{W}_i\delta_i\boldsymbol{s}_i+\varepsilon_2\gamma_2\boldsymbol{W}_i\boldsymbol{e}_{\boldsymbol{S}_{\boldsymbol{p}\boldsymbol{f}i}})\\&=\sum_{i=1}^{N}\begin{bmatrix}\boldsymbol{s}_i(t)\\\boldsymbol{e}_{\boldsymbol{S}_{pfi}}(t)\end{bmatrix}^T\begin{bmatrix}-\varepsilon_2\gamma_2\boldsymbol{W}_i\delta_i & \frac{1}{2}\varepsilon_2\gamma_2\boldsymbol{W}_i\\(\frac{1}{2}\varepsilon_2\gamma_2\boldsymbol{W}_i)^T & \boldsymbol{0}_3\end{bmatrix}\begin{bmatrix}\boldsymbol{s}_i(t)\\\boldsymbol{e}_{\boldsymbol{S}_{pfi}}(t)\end{bmatrix}\end{aligned} \tag{35}$$

Further, if condition (30) holds, we have $\dot{V}(t)<0$. Then the design NTSMFTC law can guarantee that the tracking errors of the relative position and of relative velocity tracking errors are asymptotically stable.

Step 2: The robust performance proof of the designed NTSMFTC law. Considering the performance index (31), an H_∞ performance index function is introduced as

$$J^*=\sum_{i=1}^{N}\int_0^{\infty}\boldsymbol{s}_i^T(t)\boldsymbol{s}_i(t)\mathrm{d}t-\xi\sum_{i=1}^{N}\int_0^{\infty}\boldsymbol{e}_{\boldsymbol{S}_{pfi}}^T(t)\boldsymbol{e}_{\boldsymbol{S}_{pfi}}(t)\mathrm{d}t \tag{36}$$

Then one obtains

$$\begin{aligned}J^*&=\sum_{i=1}^{N}\int_0^{\infty}\left[\boldsymbol{s}_i^T(t)\boldsymbol{s}_i(t)-\xi\boldsymbol{e}_{\boldsymbol{S}_{pfi}}^T(t)\boldsymbol{e}_{\boldsymbol{S}_{pfi}}(t)\right]\mathrm{d}t+V(t)-V(t)\\&\le\sum_{i=1}^{N}\int_0^{\infty}\left[\boldsymbol{s}_i^T(t)\boldsymbol{s}_i(t)-\xi\boldsymbol{e}_{\boldsymbol{S}_{pfi}}^T(t)\boldsymbol{e}_{\boldsymbol{S}_{pfi}}(t)\right]\mathrm{d}t+\int_0^{\infty}\dot{V}(t)\mathrm{d}t\\&=\sum_{i=1}^{N}\int_0^{\infty}\left[\boldsymbol{s}_i^T(t)\boldsymbol{s}_i(t)-\xi\boldsymbol{e}_{\boldsymbol{S}_{pfi}}^T(t)\boldsymbol{e}_{\boldsymbol{S}_{pfi}}(t)\right]\mathrm{d}t+\sum_{i=1}^{N}\int_0^{\infty}\boldsymbol{s}_i^T m_i\dot{\boldsymbol{s}}_i\mathrm{d}t\\&=\sum_{i=1}^{N}\int_0^{\infty}\left[\boldsymbol{s}_i^T(t)\boldsymbol{s}_i(t)-\xi\boldsymbol{e}_{\boldsymbol{S}_{pfi}}^T(t)\boldsymbol{e}_{\boldsymbol{S}_{pfi}}(t)+\boldsymbol{s}_i^T m_i\dot{\boldsymbol{s}}_i\right]\mathrm{d}t\end{aligned} \tag{37}$$

Under zero-initial conditions, it is defined that

$$\begin{aligned}J^*&\le\sum_{i=1}^{N}\int_0^{\infty}\big\{\boldsymbol{s}_i^T(t)\boldsymbol{s}_i(t)-\xi\boldsymbol{e}_{\boldsymbol{S}_{pfi}}^T(t)\boldsymbol{e}_{\boldsymbol{S}_{pfi}}(t)\\&\quad+\boldsymbol{s}_i^T\left[-\varepsilon_2\gamma_2\boldsymbol{W}_i\delta_i\boldsymbol{s}_i+\varepsilon_2\gamma_2\boldsymbol{W}_i\boldsymbol{e}_{\boldsymbol{S}_{pfi}}-\kappa_1\,\mathrm{sign}(\boldsymbol{s}_i)+m_i\dot{\boldsymbol{\psi}}_i\right]\big\}\mathrm{d}t\\&\le\sum_{i=1}^{N}\int_0^{\infty}\big\{\boldsymbol{s}_i^T(t)\boldsymbol{s}_i(t)-\xi\boldsymbol{e}_{\boldsymbol{S}_{pfi}}^T(t)\boldsymbol{e}_{\boldsymbol{S}_{pfi}}(t)\\&\quad+\boldsymbol{s}_i^T[-\varepsilon_2\gamma_2\boldsymbol{W}_i\delta_i\boldsymbol{s}_i+\varepsilon_2\gamma_2\boldsymbol{W}_i\boldsymbol{e}_{\boldsymbol{S}_{pfi}}]\big\}\mathrm{d}t\\&=\sum_{i=1}^{N}\int_0^{\infty}\begin{bmatrix}\boldsymbol{s}_i(t)\\\boldsymbol{e}_{\boldsymbol{S}_{pfi}}(t)\end{bmatrix}^T\begin{bmatrix}\boldsymbol{I}_3-\varepsilon_2\gamma_2\boldsymbol{W}_i\delta_i & \frac{1}{2}\varepsilon_2\gamma_2\boldsymbol{W}_i\\(\frac{1}{2}\varepsilon_2\gamma_2\boldsymbol{W}_i)^T & -\xi\boldsymbol{I}_3\end{bmatrix}\begin{bmatrix}\boldsymbol{s}_i(t)\\\boldsymbol{e}_{\boldsymbol{S}_{pfi}}(t)\end{bmatrix}\mathrm{d}t\end{aligned} \tag{38}$$

From (30), it can be deduced that $J^*\le 0$. Therefore, the robust H_∞ performance citation (31) can be obtained. This completes its proof. □

Remark 7. In the designed NTSMFTC law (29), $\boldsymbol{u}_{1i}$ is the nonlinear terminal sliding mode term, $\boldsymbol{u}_{2i}$ is the feedforward feedback term, $\boldsymbol{u}_{3i}$ the synthesized disturbance compensation term. The prescribed H_∞ performance constraint (31) is introduced to attenuate the influence of disturbance reconstruction error $\boldsymbol{e}_{\boldsymbol{S}_{pfi}}$. Therefore, the proposed robust NTSMFTC law (29) can guarantee the convergence errors of relative position and relative velocity with prescribed H_∞ performance constraint during formation reconfiguration.

Remark 8. To eliminate the chattering phenomenon that results from the repeated switching on the sliding mode surface in the convergence process, the following saturation function sat(•) can be used to replace the sign function sign(•) in (29)

$$\mathrm{sat}(s_{ik})=\begin{cases}1 & s_{ik}>\Delta\\-1 & s_{ik}<-\Delta\\s_{ik}/\Delta & |s_{ik}|\le\Delta\end{cases} \tag{39}$$

where s_{ik} is the element of $\boldsymbol{s}_i$, and Δ is a known constant satisfying $\Delta>0$.

Remark 9. From the NTSM surface (27) and the NTSMFTC law (29), it can be noted that the relative information between the leader spacecraft and all the follower spacecrafts is only required. Compared with the collision avoidance formation configuration approaches [11,15], the relative information between all the follower spacecraft are not required in the proposed NTSMFTC approach. In other words, it is not necessary for the communication topology between all the follower spacecrafts. Therefore, the proposed NTSMFTC approach can reduce the communication burden in the considered SFF systems.

Remark 10. From (30), it can be seen that the time-varying term $\boldsymbol{W}_i$ is a function of relative velocity error $\boldsymbol{e}_{\boldsymbol{v}i}$. Therefore, sliding mode parameter δ_i can be adaptively updated by calculating (30) to guarantee the prescribed H_∞ performance index (31). In

other words, to guarantee the robustness against the disturbance reconstruction error, time-varying parameter $\boldsymbol{\delta}_i$ is required in the proposed NTSMFTC approach. A local minimum ξ can be obtained through solving (30) using the solver *mincx* in the MATLAB/LMI toolbox. Alternatively, parameter $\boldsymbol{\delta}_i$ can be computed using the solver *feasp* with an appropriate H_∞ performance index ξ.

Following Theorem 2, a full design procedure for the presented NTSMFTC law is outlined as follows,

Design procedure for the presented NTSMFTC law	
1.	Select the weight coefficient Υ for the APF satisfying $\Upsilon > 0$.
2.	Choose gain parameters ε_1 and ε_2.
3.	Choose exponential parameters γ_1 and γ_2.
4.	Choose appropriate positive scalar κ_1 according to (25).
5.	Select positive scalar Δ for saturation function in the form of (39).
6.	Compute $\boldsymbol{R}_i$ and $\boldsymbol{W}_i$ according to the position tracking error $\boldsymbol{e}_{\rho i}$ and velocity tracking error $\boldsymbol{e}_{\boldsymbol{v}i}$ respectively.
7.	Choose an appropriate H_∞ performance index ξ, and solve (30) to obtain matrix $\boldsymbol{\delta}_i$ by using Matlab/LMI toolbox.

5. Simulation results

In this section, a numerical example on a satellite formation flying system is provided to demonstrate the effectiveness and superiority of the proposed performance guaranteed formation reconfiguration FTC approach for multi-spacecraft system.

5.1. Simulation parameters

The considered satellite formation flying system is composed of a virtual leader and three follower satellites. The mass of each satellite is assumed to be 135 kg and the virtual leader satellite is assumed to be flying in a near circular orbit with $a = 7000$ km. The space perturbation [37] is chosen as

$$\boldsymbol{d}_i = 10^{-3} \bullet [-1.025, 6.248, -2.415]^T \sin\left(2\pi\sqrt{\frac{\mu}{a^3}}t\right)$$

In addition, it considers that there exist small thruster faults including abrupt constant fault and time-varying fault. The specific thruster fault scenarios are assumed as follows,

$$f_x(t) = \begin{cases} 0 & t \le 1000\ \text{s} \\ 0.01 & t \ge 1000\ \text{s} \end{cases}, \qquad f_y(t) = 0,$$

$$f_z(t) = \begin{cases} 0 & t \le 1500\ \text{s} \\ 0.015\sin(0.01t + \frac{\pi}{4}) & t \ge 1500\ \text{s} \end{cases}$$

In the simulation, the simulation step is set to be 0.005 s. The estimated initial system state $\hat{\boldsymbol{q}}_i(0)$ is set to be zero vector. The initial states and the desired relative position of the three follower satellites are assumed as follows,

$$\begin{cases} \boldsymbol{q}_1(0) = [200\sqrt{2}, 400, 250, 0, -0.5, 0]^T \\ \boldsymbol{q}_2(0) = [0, -350, 50, -0.25, 0, -0.25]^T \\ \boldsymbol{q}_3(0) = [-200\sqrt{2}, 0, -250, 0, -0.5, 0]^T \end{cases},$$

$$\boldsymbol{\rho}_{id} = \begin{bmatrix} 400\sqrt{2}\cos(nt + i \bullet \frac{2\pi}{3}) \\ -250\sin(nt + i \bullet \frac{2\pi}{3}) \\ 400\cos(nt + i \bullet \frac{2\pi}{3}) \end{bmatrix} \text{m}$$

To avoid collision between each satellite in multi-satellite formation system, the predetermined safe distance is assumed as $M_d = 300$ m.

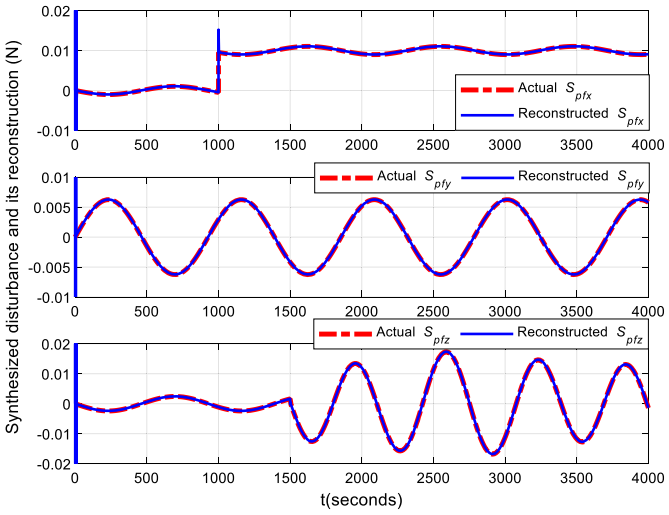

Fig. 4. The reconstructed signals of the synthesized disturbance with different fault scenarios.

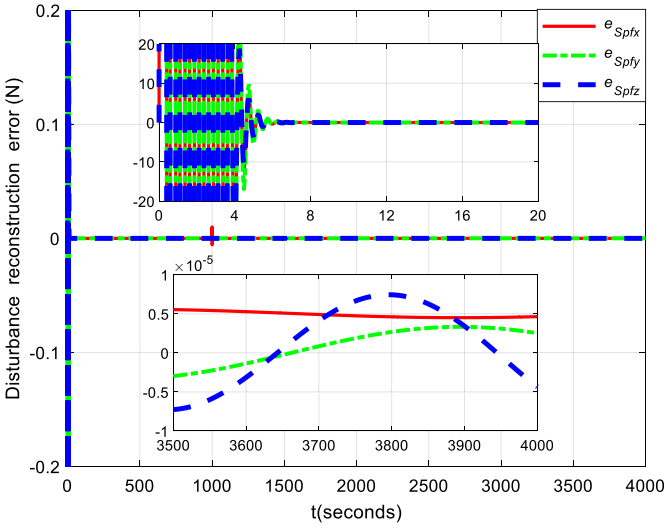

Fig. 5. The reconstruction error of the synthesized disturbance.

5.2. NILDO-based synthesized disturbance reconstruction

In this simulation, the disturbance reconstruction for the follower satellite 1 is taken as an example to illustrate the superior performance of the designed NILDO. Firstly, one obtains $\boldsymbol{Q}_1 = \text{diag}\{0.999, 0.999, 0.999\}$ by choosing parameter $\vartheta_1 = 0.0002$. For the good transient performance, all poles of matrix $\boldsymbol{A} - \boldsymbol{L}_1\boldsymbol{C}$ can be located in the stability region $\Re(-3, 2)$ [39]. Select parameters $L_{g1} = 0.01$ and $\varpi = 10^{-8}$, then solve (21) and (22) by using the Matlab/LMI toolbox yields

$$\boldsymbol{L}_1 = \begin{bmatrix} 4.1149 & 0 & 0 & 1.0000 & 0 & 0 \\ 0 & 4.1149 & 0 & 0 & 1.0000 & 0 \\ 0 & 0 & 4.1149 & 0 & 0 & 1.0000 \\ 0 & 0 & 0 & 4.1149 & 0.0022 & 0 \\ 0 & 0 & 0 & -0.0022 & 4.1149 & 0 \\ 0 & 0 & 0 & 0 & 0 & 4.1149 \end{bmatrix}$$

$$\boldsymbol{K}_1 = \begin{bmatrix} 0 & 0 & 0 & 109.9042 & 0 & 0 \\ 0 & 0 & 0 & 0 & 109.9044 & 0 \\ 0 & 0 & 0 & 0 & 0 & 109.9045 \end{bmatrix}$$

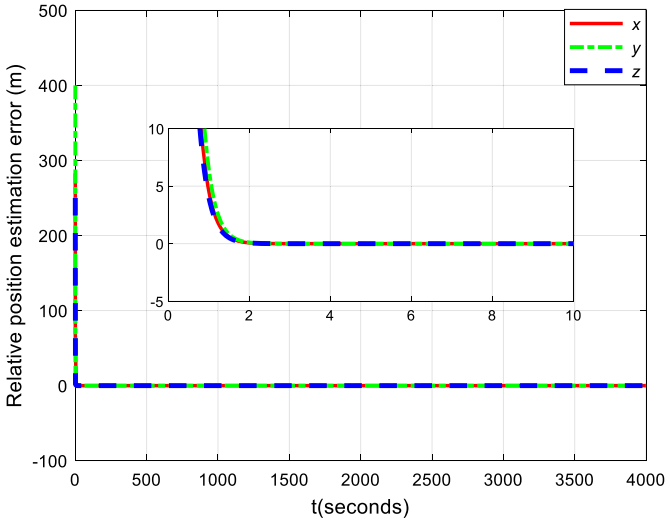

Fig. 6. The estimation error of relative position.

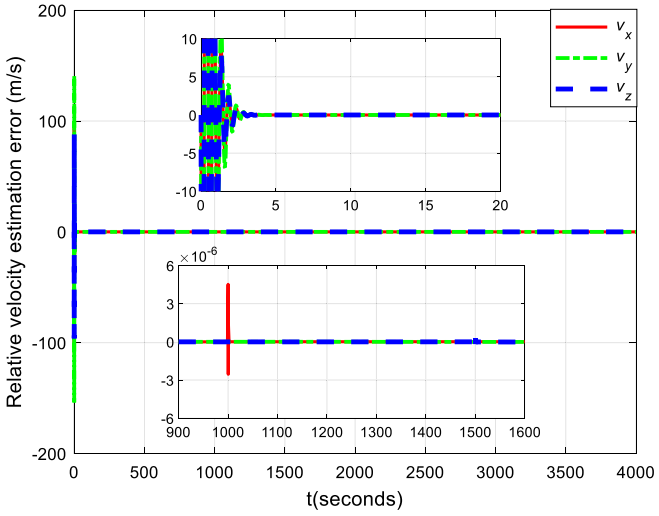

Fig. 7. The estimation error of relative velocity.

In the simulation, the learning interval τ is selected to be 0.005 s. Simulation results on NILDO-based synthesized disturbance reconstruction and time responses of the reconstruction error are respectively provided in Figs. 4–5. It can be observed that the designed NILDO can provide fast and accurate reconstruction of synthesized disturbance even considering abrupt constant fault and time-varying fault. It is noteworthy that the reconstruction signal in the y-axis accurately tracks the space perturbation when considering no thruster fault in this axis. In addition, Figs. 6–7 clearly illustrate the estimation errors of the relative position and the relative velocity, respectively. It can be seen that the estimation errors can fast converge to small neighborhoods of zero in different fault scenarios. It implies the designed NILDO can accurately estimate the relative position and relative velocity for the leader-follower satellite formation system. Therefore, it can be concluded that the designed NILDO can not only reconstruct the synthesized disturbance, but also estimate the system state including the relative position and relative velocity for the leader-follower SFF system.

To illustrate the superiority of the presented disturbance reconstruction method, a comparison between the proposed NILDO and the existing NDO proposed in [22] is detailed provided under the same simulation conditions. Comparative results on disturbance reconstruction in the three axes are demonstrated in Fig. 8–10. It is obvious that, compared with the existing NDO, the designed NILDO has faster convergence property and more accurate reconstruction of the synthesized disturbance. It is mainly because that constant or slow-varying disturbances are theoretically considered in the existing NDO [22]. The disturbance reconstruction errors of NILDO and NDO in the three axes are provided in Table 1. It can be found that, reconstruction accuracy of the designed NILDO is one order of magnitude larger than that of the existing NDO [22]. Therefore, all the simulation results strongly validate the effectiveness and superiority of the proposed disturbance reconstruction approach.

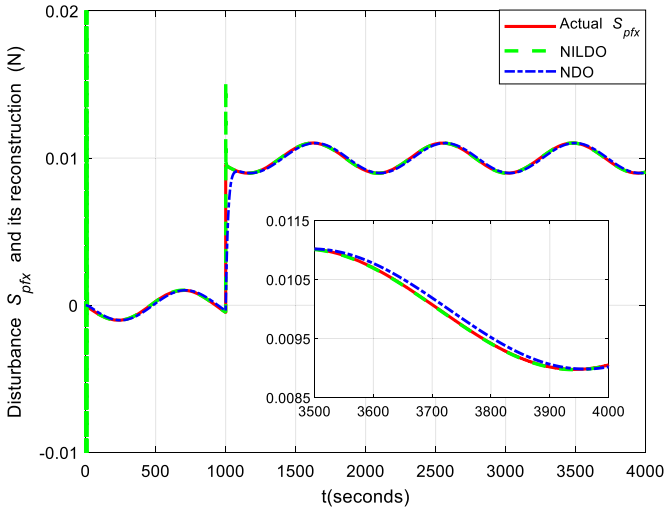

Fig. 8. Disturbance-reconstructing results in the x-axis of the designed NILDO and the existing NDO [22].

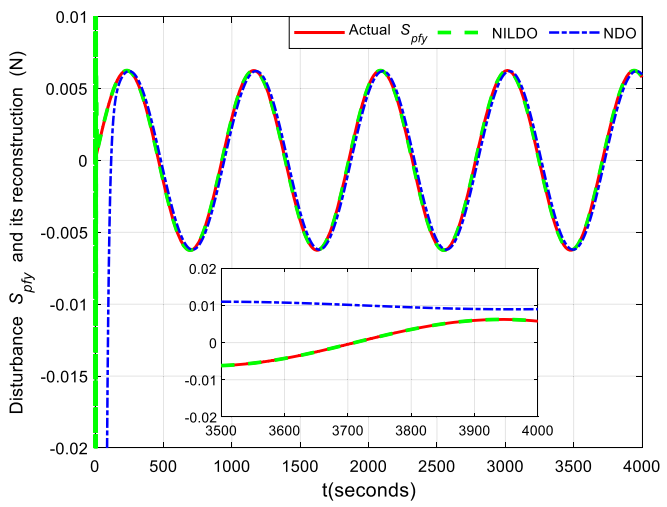

Fig. 9. Disturbance-reconstructing results in the y-axis of the designed NILDO and the existing NDO [22].

Table 1
The comparison results of disturbance reconstruction error.

	x-axis (N)	y-axis (N)	z-axis (N)
NDO [22]	1.164×10^{-4}	7.094×10^{-4}	2.695×10^{-4}
NILDO	5.595×10^{-6}	3.331×10^{-6}	9.709×10^{-6}

5.3. NTSMFTC-based multi-spacecraft formation reconfiguration

In this subsection, an exponential APF-based robust NTSMFTC law is designed and the related simulation is provided in detail.

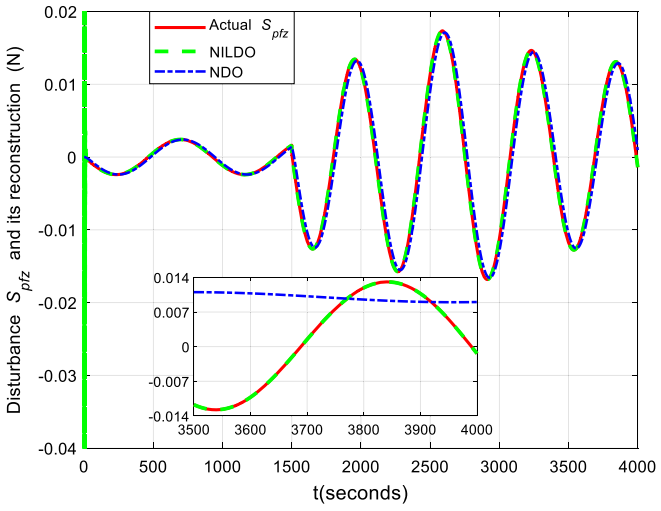

Fig. 10. Disturbance-reconstructing results in the z-axis of the designed NILDO and the existing NDO [22].

Table 2
The parameters of the NTSMFTC law.

Parameters	Values	Parameters	Values
Υ	80	Δ	0.05
ξ	1	κ_1	3000
γ_1	2	ε_1	0.0062
γ_2	9/7	ε_2	0.0062

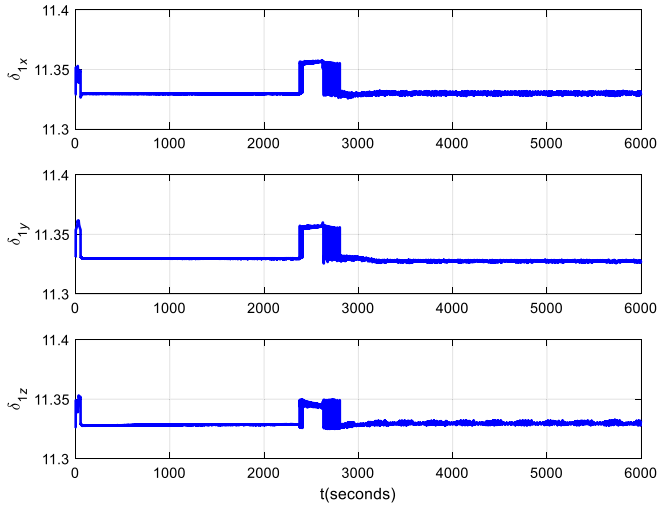

Fig. 11. The time response curve of the time-varying matrix δ_1.

Following the design procedure of the NTSMFTC law, its control parameters are computed and given in Table 2. The time response curve of matrix δ_1 is shown in Fig. 11. The computation results of matrices δ_2 and δ_3 are similar to those of matrix δ_1, and they are thus omitted here.

Simulation results on NTSMFTC law-based formation reconfiguration with collision avoidance are demonstrated in Figs. 12–15. Fig. 12 illustrates the distances between three follower satellites during the spacecraft formation reconfiguration. It can be seen that the distance between any two follower satellites in formation satisfies the predetermined safe distance requirement such that collision avoidance can be achieved in the process of formation reconfiguration. Figs. 13–15 clearly illustrate three-dimensional trajectory, two-dimensional trajectory in the *xoy* plane and in the *yoz* plane respectively. From Figs. 13–15, it can be seen that three

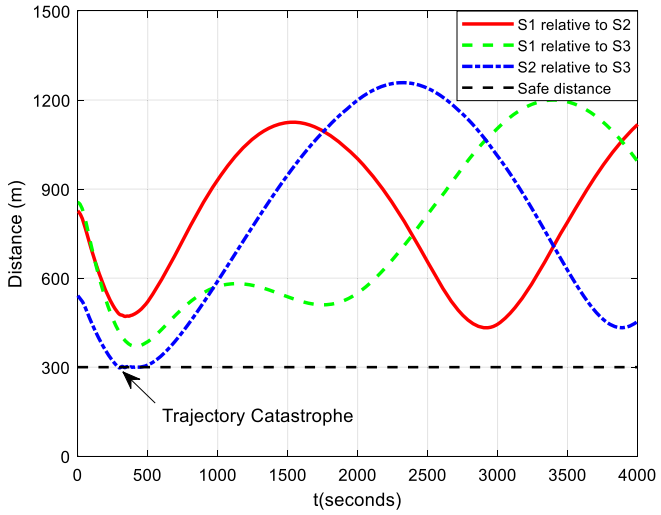

Fig. 12. Distances between three follower satellites during formation reconfiguration (Satellite 1:S1, Satellite 2:S2, Satellite 3:S3).

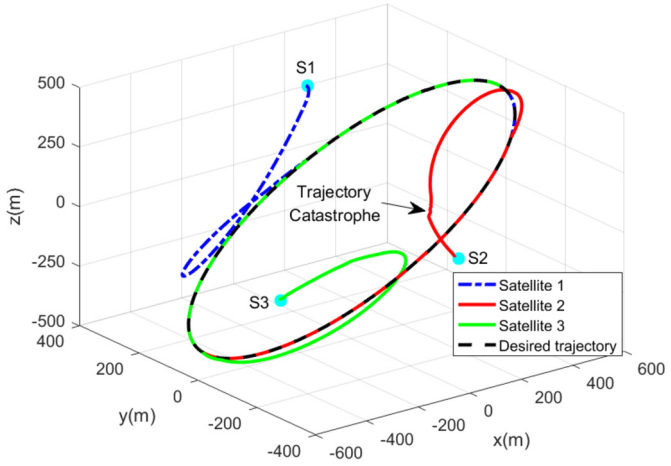

Fig. 13. Three-dimensional reconfiguration trajectory of multi-satellite formation.

follower satellites converge to the desired formation configuration accurately, and trajectory catastrophes of the second and third follower satellites occur in the influence of exponential APF when the distance between them gets close to 300 m.

To demonstrate the superiority of the presented robust NTSMFTC law, simulation results on the position tracking error under the NTSMFTC law, the LSMC [19] and the NTSMC [26] are given in Figs. 16–18. In addition, the relative position tracking error and its relative percentage are respectively provided in Table 3 and Table 4. From Figs. 16–18, it is clearly seen that the proposed NTSMFTC method has significant advantages than the LSMC [19] and the NTSMC [26] on the convergence speed and the relative position tracking error. From the Table 3 and Table 4, it can be found that, the relative position tracking accuracy under the proposed NTSMFTC is at least two orders of magnitude higher than that under the LSMC. In addition, the tracking accuracy under the NTSMFTC is also higher than that under the NTSMC. These competitive results for the proposed NTSMFTC are obtained mainly because the synthesized disturbance is accurately reconstructed using the proposed NILDO and is compensated in the NTSMFTC law.

To demonstrate the prescribed H_∞ performance index $J^* \leq 0$ can be guaranteed, the time response of the term $J = \sum_{i=1}^{N} \boldsymbol{s}_i^T(t)\boldsymbol{s}_i(t) - \xi \sum_{i=1}^{N} \boldsymbol{e}_{\boldsymbol{S}_{\mathbf{pfi}}}^T(t)\boldsymbol{e}_{\boldsymbol{S}_{\mathbf{pfi}}}$ for J^* is shown in Fig. 19.

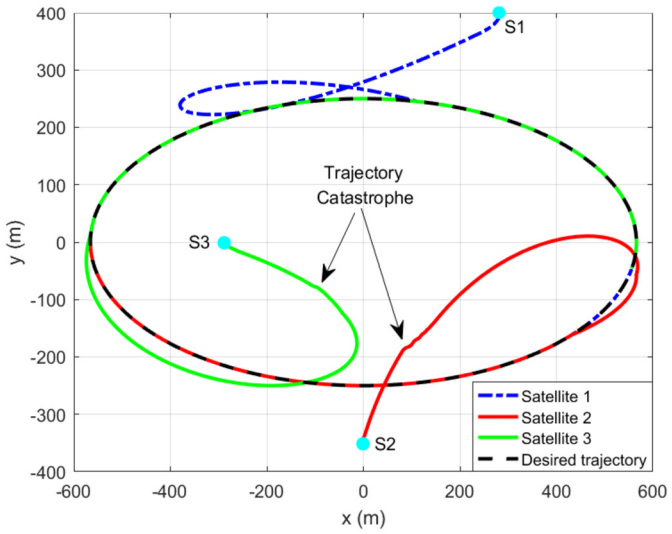

Fig. 14. Two-dimensional reconfiguration trajectory in *xoy* plane of multi-satellite formation.

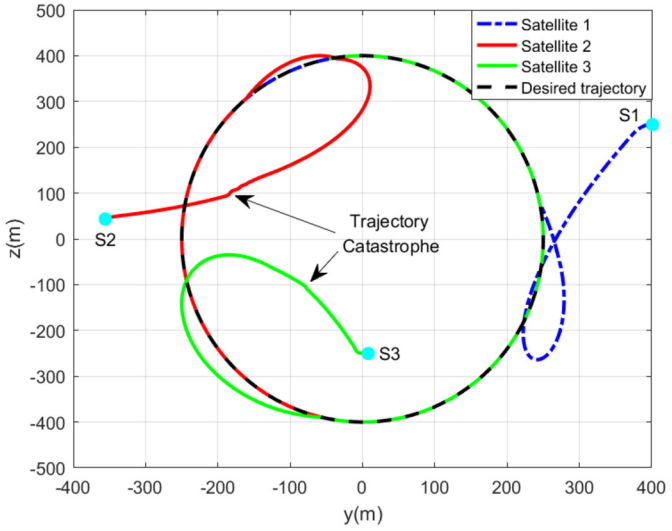

Fig. 15. Two-dimensional reconfiguration trajectory in *yoz* plane of multi-satellite formation.

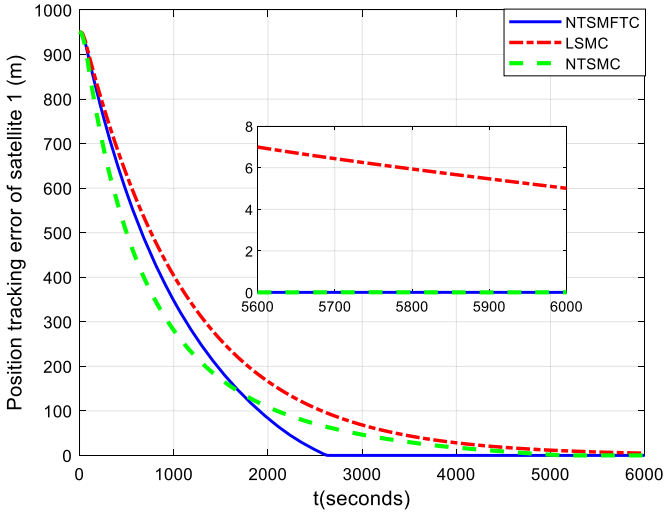

Fig. 16. The position tracking error of the follower satellite 1 for formation reconfiguration.

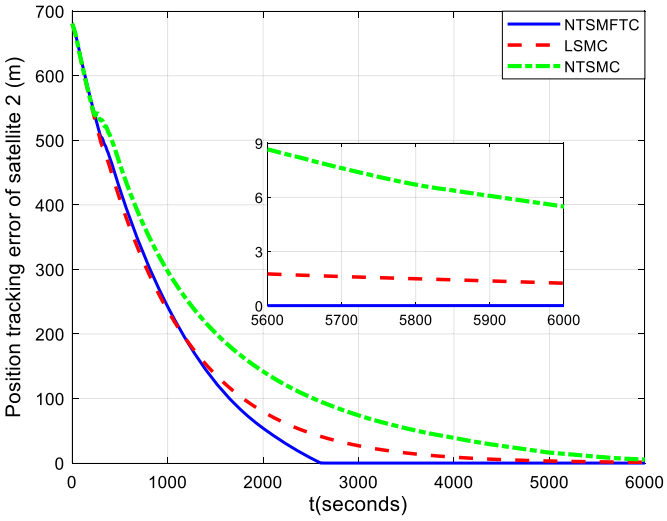

Fig. 17. The position tracking error of the satellite 2 for formation reconfiguration.

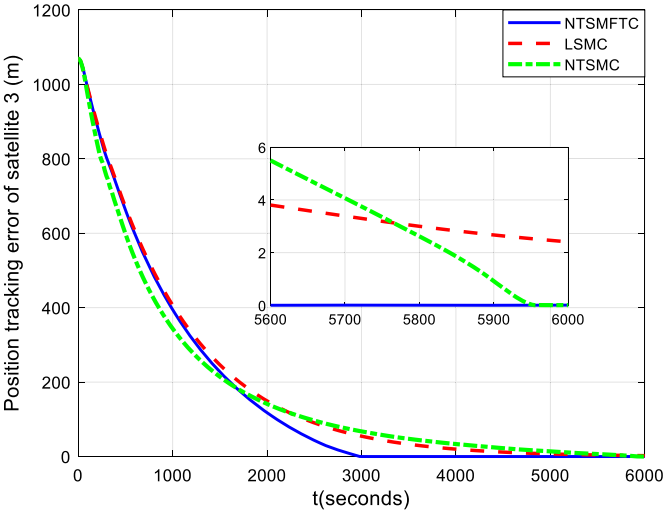

Fig. 18. The position tracking error of the satellite 3 for formation reconfiguration.

Table 3
The comparison results of the relative position tracking error.

Error term	NTSMFTC	LSMC [19]	NTSMC [26]
$x_1 - x_{1d}$ (m)	0.0029	3.3166	0.0059
$y_1 - y_{1d}$ (m)	0.0001	2.9789	0.0005
$z_1 - z_{1d}$ (m)	−0.0055	2.2867	−0.0060
$x_2 - x_{2d}$ (m)	0.0042	0.8269	0.0054
$y_2 - y_{2d}$ (m)	0.0001	−0.8444	−5.4860
$z_2 - z_{2d}$ (m)	−0.0052	0.3899	−0.0082
$x_3 - x_{3d}$ (m)	0.0030	−1.7667	0.0051
$y_3 - y_{3d}$ (m)	0.0001	0.0165	0.0005
$z_3 - z_{3d}$ (m)	−0.0078	−1.6389	−0.0096

Table 4
The comparison results of relative error term for the relative position tracking.

Relative Error term	NTSMFTC	LSMC [19]	NTSMC [26]
$\lvert x_1 - x_{1d}\rvert / x_{1d}$	0.0008%	0.9017%	0.0016%
$\lvert y_1 - y_{1d}\rvert / y_{1d}$	0.0001%	1.5700%	0.0003%
$\lvert z_1 - z_{1d}\rvert / z_{1d}$	0.0021%	0.8800%	0.0023%
$\lvert x_2 - x_{2d}\rvert / x_{2d}$	0.0022%	0.4400%	0.0029%
$\lvert y_2 - y_{2d}\rvert / y_{2d}$	0.0001%	0.3600%	2.3300%
$\lvert z_2 - z_{2d}\rvert / z_{2d}$	0.0039%	0.2900%	0.0062%
$\lvert x_3 - x_{3d}\rvert / x_{3d}$	0.0005%	0.3200%	0.0010%
$\lvert y_3 - y_{3d}\rvert / y_{3d}$	0.0002%	0.0360%	0.0011%
$\lvert z_3 - z_{3d}\rvert / z_{3d}$	0.0020%	0.4200%	0.0024%

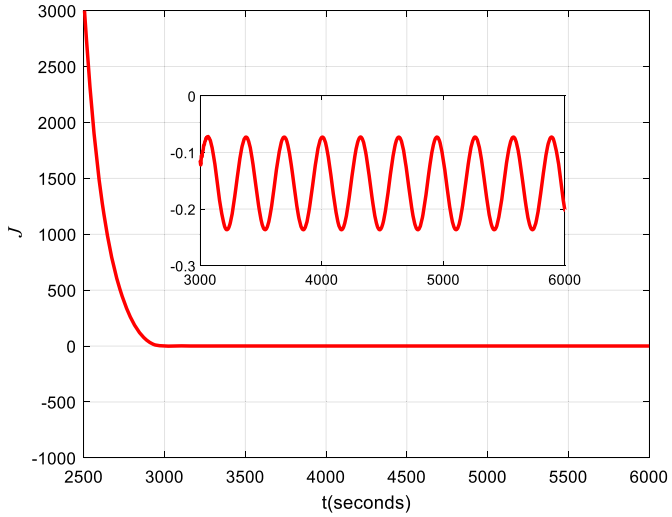

Fig. 19. The time response curve of the term J.

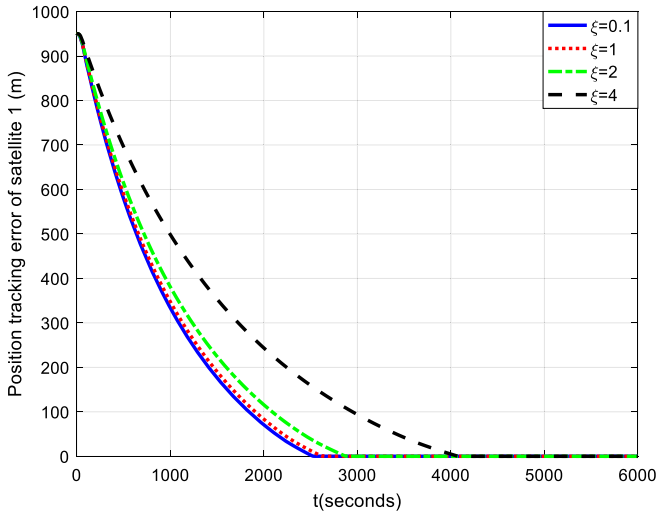

Fig. 20. The position tracking error of the satellite 1 for formation reconfiguration in different values of ξ.

It can be observed that $J < 0$ always holds after the three satellites converge to their respective desired positions. It signifies that the prescribed H_∞ performance can be guaranteed under the NTSMFTC law. To illustrate the influence of the performance parameter ξ, the convergence curves of the position tracking error of satellite 1 when considering different values of parameter ξ are shown in Fig. 20. It can be observed that, as the value of parameter ξ decreases, the convergence speed of the relative position tracking error becomes quickly. In particular, parameter ξ decreases to a very small value, the change of the convergence speed is very small. It is mainly because parameter ξ is chosen to be close to its local minima. Therefore, it can be concluded that the proposed NILDO-based NTSMFTC approach can achieve robust and accurate formation configuration with collision avoidance ability and fault-tolerant ability.

6. Conclusion

This paper has investigated the issue of NILDO-based performance guaranteed formation reconfiguration control for a class of multi-spacecraft system subjects to space perturbations and thruster faults. An NILDO has been presented for precise reconstruction of the synthesized disturbances. Compared with the existing NDO, the proposed NILDO has higher reconstruction accuracy on time-varying disturbances. Further, an NTSMFTC approach with exponential APF has been designed for closed-loop SFF system such that accurate and fast formation reconfiguration with collision avoidance and prescribed H_∞ performance has been guaranteed. The proposed NTSMFTC approach has one order of magnitude performance improvement over the conventional LSMC approach while it has higher control accuracy than the NTSMC approach. In addition, it also has faster convergence speed than these two control approaches. Finally, through the numerical simulations, the effectiveness and superiority of the proposed approaches have been substantiated.

We would like to point out that, constrained communication in the spacecraft formation control is another important issue to be solved, especially in the large-scale spacecraft formation. Based on the proposed approaches, event-triggered based spacecraft fault-tolerant formation reconfiguration control under constrained communication and collision avoidance will be investigated in our further research work.

Declaration of competing interest

The authors declare the following financial interests/personal relationships which may be considered as potential competing interests:

Qingxian Jia reports article publishing charges and equipment, drugs, or supplies were provided by National Natural Science Foundation of China. Yunhua Wu reports article publishing charges and equipment, drugs, or supplies were provided by National Natural Science Foundation of China. Qingxian Jia reports article publishing charges, equipment, drugs, or supplies, and statistical analysis were provided by High-level Innovation and Entrepreneurship Talents Introduction Program of Jiangsu Province of China. Yule Gui reports writing assistance was provided by Nanjing University of Aeronautics and Astronautics.

Data availability

No data was used for the research described in the article.

Acknowledgements

This work is partially supported by National Natural Science Foundation of China (Grant No. 61703276, 61973153), High-level Innovation and Entrepreneurship Talents Introduction Pro-

gram of Jiangsu Province of China ((2019)30574) and Postgraduate Research & Practice Innovation Program of NUAA (Grant No. xcxjh20211503).

Appendix A

Annotated table	
SFF	Spacecraft Formation Flying
FTC	Fault-Tolerant Control
APF	Artificial Potential Function
LSMC	Linear Sliding Mode Control
NTSMC	Nonsingular Terminal Sliding Mode Control
NTSMFTC	Nonsingular Terminal Sliding Mode Fault-Tolerant Control
ILO	Iterative Learning Observer
NDO	Nonlinear Disturbance Observer
NILDO	Nonlinear Iterative Learning Disturbance Observer
LMI	Linear Matrix Inequality
$\boldsymbol{\rho}_i$	Relative Position Vector
$\boldsymbol{v}_i$	Relative Velocity Vector
$\boldsymbol{d}_i$	Space Perturbation Vector
$\boldsymbol{f}_i$	Thruster Fault Vector
$\boldsymbol{u}_i$	Control Force Vector
$\boldsymbol{S}_{pfi}$	Synthesized Disturbance Vector
$\hat{\boldsymbol{S}}_{pfi}$	Reconstructed Synthesized Disturbance Vector
$e_{\boldsymbol{S}_{pfi}}$	Disturbance Reconstruction Error
d_{ij}	Space Distance between ith Spacecraft and jth Spacecraft
$\boldsymbol{\rho}_{id}$	Desired Relative Position Vector
$\boldsymbol{\delta}_i$	Controller Parameter
$\boldsymbol{s}_i$	Sliding Mode Surface
$\boldsymbol{R}_i$	Matrix Related to Position Error
$\boldsymbol{W}_i$	Matrix Related to Velocity Error
Subscript i	Spacecraft Designating Number

References

[1] D. Wang, B. Wu, E.K.P. Chung, Satellite Formation Flying, Springer, Singapore, 2017.
[2] S. Mathavaraj, R. Padhi, Satellite Formation Flying, Springer, New Delhi, India, 2021.
[3] D.P. Scharf, F.Y. Hadaegh, S.R. Ploen, A survey of spacecraft formation flying guidance and control. Part II: control, in: Proceedings of the 2004 American Control Conference, vol. 4, IEEE, 2004, pp. 2976–2985.
[4] G. Liu, S. Zhang, A survey on formation control of small satellites, Proc. IEEE 106 (2018) 440–457.
[5] G. Di Mauro, M. Lawn, R. Bevilacqua, Survey on guidance navigation and control requirements for spacecraft formation-flying missions, J. Guid. Control Dyn. 41 (3) (2018) 581–602.
[6] K. Raigoza, T. Sands, Autonomous trajectory generation comparison for de-orbiting with multiple collision avoidance, Sensors 22 (18) (2022) 7066.
[7] N. Zhou, Y. Xia, Coordination control design for formation reconfiguration of multiple spacecraft, IET Control Theory Appl. 9 (15) (2015) 2222–2231.
[8] Z. Wang, Y. Xu, C. Jiang, et al., Self-organizing control for satellite clusters using artificial potential function in terms of relative orbital elements, Aerosp. Sci. Technol. 84 (2019) 799–811.
[9] S. Renevey, D.A. Spencer, Establishment and control of spacecraft formations using artificial potential functions, Acta Astronaut. 162 (2019) 314–326.
[10] Y. Wang, X. Chen, D. Ran, et al., Spacecraft formation reconfiguration with multi-obstacle avoidance under navigation and control uncertainties using adaptive artificial potential function method, Astrodynamics 4 (1) (2020) 41–56.
[11] M. Zhuang, T.A.N. Liguo, L.I. Kehang, et al., Fixed-time position coordinated tracking control for spacecraft formation flying with collision avoidance, Chin. J. Aeronaut. 34 (11) (2021) 182–199.
[12] J. Hwang, J. Lee, C. Park, Collision avoidance control for formation flying of multiple spacecraft using artificial potential field, Adv. Space Res. 69 (5) (2022) 2197–2209.
[13] C. Lippe, S. D'Amico, Safe, delta-v-efficient spacecraft swarm reconfiguration using Lyapunov stability and artificial potentials, J. Guid. Control Dyn. 45 (2) (2022) 213–231.
[14] M. Zhuang, L. Tan, K. Li, et al., Fixed-time formation control for spacecraft with prescribed performance guarantee under input saturation, Aerosp. Sci. Technol. 119 (2021) 107176.
[15] C. Wei, X. Wu, B. Xiao, et al., Adaptive leader-following performance guaranteed formation control for multiple spacecraft with collision avoidance and connectivity assurance, Aerosp. Sci. Technol. 120 (2022) 107266.
[16] Q. Hu, W. Chen, L. Guo, et al., Adaptive fixed-time attitude tracking control of spacecraft with uncertainty-rejection capability, IEEE Trans. Syst. Man Cybern. Syst. 52 (7) (2022) 4634–4647.
[17] X. Shao, Q. Hu, Z. Zhu, et al., Fault-tolerant reduced-attitude control for spacecraft constrained boresight reorientation, J. Guid. Control Dyn. (2022) 1–15.
[18] Y. Gui, Q. Jia, H. Li, et al., Reconfigurable fault-tolerant control for spacecraft formation flying based on iterative learning algorithms, Appl. Sci. 12 (5) (2022) 2485.
[19] L. Cao, X. Chen, Input–output linearization minimum sliding-mode error feedback control for spacecraft formation with large perturbations, Proc. Inst. Mech. Eng., G J. Aerosp. 229 (2) (2015) 352–368.
[20] P. Li, Z. Liu, C. He, et al., Distributed adaptive fault-tolerant control for spacecraft formation with communication delays, IEEE Access 8 (2020) 118653–118663.
[21] K. Wang, T. Meng, W. Wang, et al., Finite-time extended state observer based prescribed performance fault tolerance control for spacecraft proximity operations, Adv. Space Res. 70 (2022) 1270–1284.
[22] D. Lee, Nonlinear disturbance observer-based robust control for spacecraft formation flying, Aerosp. Sci. Technol. 76 (2018) 82–90.
[23] C. Du, C. Yang, F. Li, et al., Design and implementation of observer-based sliding mode for underactuated rendezvous system, IEEE Trans. Syst. Man Cybern. Syst. 51 (10) (2019) 6003–6014.
[24] X. Zhu, Z. Zhu, J. Chen, Dual quaternion-based adaptive iterative learning control for flexible spacecraft rendezvous, Acta Astronaut. 189 (2021) 99–118.
[25] Q. Jia, W. Chen, Y. Zhang, et al., Fault reconstruction for continuous-time systems via learning observers, Asian J. Control 18 (2) (2016) 549–561.
[26] Y. Wang, W. Yao, X. Chen, et al., Novel Gaussian mixture model based nonsingular terminal sliding mode control for spacecraft close-range proximity with complex shape obstacle, Proc. Inst. Mech. Eng., G J. Aerosp. 236 (3) (2022) 517–526.
[27] N. Zhou, R. Chen, Y. Xia, et al., Neural network–based reconfiguration control for spacecraft formation in obstacle environments, Int. J. Robust Nonlinear Control 28 (6) (2018) 2442–2456.
[28] F. Nemati, S.M.S. Hamami, A. Zemouche, A nonlinear observer-based approach to fault detection, isolation and estimation for satellite formation flight application, Automatica 107 (2019) 474–482.
[29] K. Shi, C. Liu, J.D. Biggs, et al., Observer-based control for spacecraft electromagnetic docking, Aerosp. Sci. Technol. 99 (2020) 105759.
[30] Q. Hu, X. Shao, Smooth finite-time fault-tolerant attitude tracking control for rigid spacecraft, Aerosp. Sci. Technol. 55 (2016) 144–157.
[31] Q. Jia, H. Li, X. Chen, et al., Observer-based reaction wheel fault reconstruction for spacecraft attitude control systems, Aircr. Eng. Aerosp. Technol. 91 (10) (2019) 1268–1277.
[32] J. Zhu, G. Yang, H. Wang, et al., Fault estimation for a class of nonlinear systems based on intermediate estimator, IEEE Trans. Autom. Control 61 (9) (2015) 2518–2524.
[33] Z. Peng, D. Wang, H. Zhang, Cooperative tracking and estimation of linear multi-agent systems with a dynamic leader via iterative learning, Int. J. Control 87 (6) (2014) 1163–1171.
[34] Q. Hu, X. Zhang, G. Niu, Observer-based fault tolerant control and experimental verification for rigid spacecraft, Aerosp. Sci. Technol. 92 (2019) 373–386.
[35] X. Zhu, J. Chen, Z. Zhu, Adaptive learning observer for spacecraft attitude control with actuator fault, Aerosp. Sci. Technol. 108 (2021) 106389.
[36] T. Cao, H. Gong, P. Cheng, et al., A novel learning observer-based fault-tolerant attitude control for rigid spacecraft, Aerosp. Sci. Technol. 128 (2022) 107751.
[37] Q. Hu, H. Dong, Y. Zhang, et al., Tracking control of spacecraft formation flying with collision avoidance, Aerosp. Sci. Technol. 42 (2015) 353–364.
[38] X. Lin, X. Shi, S. Li, et al., Nonsingular fast terminal adaptive neuro-sliding mode control for spacecraft formation flying systems, Complexity 2020 (2020).
[39] G. Garcia, J. Bernussou, Pole assignment for uncertain systems in a specified disk by state feedback, IEEE Trans. Autom. Control 40 (1) (1995) 184–190.